

Annual Review of Earth and Planetary Sciences

The 2018 Eruption of Kīlauea: Insights, Puzzles, and Opportunities for Volcano Science

Kyle R. Anderson,¹ Thomas Shea,² Kendra J. Lynn,³ Emily K. Montgomery-Brown, Donald A. Swanson, Matthew R. Patrick,³ Brian R. Shiro,⁵ and Christina A. Neal⁶

Annu. Rev. Earth Planet. Sci. 2024. 52:1.1-1.39

The Annual Review of Earth and Planetary Sciences is online at earth.annualreviews.org

https://doi.org/10.1146/annurev-earth-031621-

This is a work of the US Government and is not subject to copyright protection in the United States

Keywords

basaltic volcanism, caldera collapse, magma system, Hawai'i volcano, rift zone, tephra eruption

Abstract

The science of volcanology advances disproportionately during exceptionally large or well-observed eruptions. The 2018 eruption of Kīlauea Volcano (Hawai'i) was its most impactful in centuries, involving an outpouring of more than one cubic kilometer of basalt, a magnitude 7 flank earthquake, and the volcano's largest summit collapse since at least the nineteenth century. Eruptive activity was documented in detail, yielding new insights into large caldera-rift eruptions; the geometry of a shallow magma storage-transport system and its interaction with rift zone tectonics; mechanisms of basaltic tephra-producing explosions; caldera collapse mechanics; and the dynamics of fissure eruptions and high-volume lava flows. Insights are broadly applicable to a range of volcanic systems and should reduce risk from future



¹USGS Volcano Science Center, Moffett Field, California, USA; email: kranderson@usgs.gov

²Department of Earth Sciences, University of Hawai'i at Mānoa, Honolulu, Hawai'i, USA

³USGS Hawaiian Volcano Observatory, Hilo, Hawai'i, USA

⁴USGS Cascades Volcano Observatory, Vancouver, Washington, USA

⁵USGS Geologic Hazards Science Center, Golden, Colorado, USA

⁶USGS Volcano Science Center, Anchorage, Alaska, USA

eruptions. Multidisciplinary collaboration will be required to fully leverage the diversity of monitoring data to address many of the most important outstanding questions.

- Unprecedented observations of a caldera collapse and coupled rift zone eruption yield new opportunities for advancing volcano science.
- Magma flow to a low-elevation rift zone vent triggered quasi-periodic step-like collapse of a summit caldera, which pressurized the magma system and sustained the eruption.
- Kīlauea's magmatic-tectonic system is tightly interconnected over tens of kilometers, with complex feedback mechanisms and interrelated hazards over widely varying time scales.
- The eruption revealed magma stored in diverse locations, volumes, and compositions, not only beneath the summit but also within the volcano's most active rift zone.

1. INTRODUCTION

Kīlauea is one of the world's most active and closely monitored volcanoes. Its 2018 eruption was its largest and most impactful in 200 years, and one of the most costly volcanic disasters in US history (Williams et al. 2020). The detail and breadth of monitoring observations, spanning the volcanic system from summit to rift zone vents 40 km distant, were unprecedented for an eruption of this scale. Of the handful of caldera collapses observed on Earth in the last century, Kīlauea's is by far the best documented.

Monitoring data were used during the eruption to infer and communicate hazards to the public (Neal et al. 2019, Neal & Anderson 2020) and now present what may be a once-in-a-generation opportunity to improve understanding of Kīlauea Volcano, with broad implications for basaltic volcanism, summit-rift eruptions, ocean island volcanoes, and caldera collapses—in keeping with a long tradition in which Kīlauea has served as a natural laboratory for developing volcanological techniques and theories (Tilling et al. 2014, Garcia 2015).

In this review, after providing a brief introduction to Kīlauea and the 2018 eruption sequence, we summarize the main findings from the first five years of research efforts, describe how the eruption has informed and changed our ideas, discuss open questions, and identify avenues for future work. Our focus is on the magmatic-tectonic system, as characterized by a synthesis of diverse interdisciplinary observations, and we touch only briefly on monitoring techniques, hazards, and human and environmental impacts. However, we present some references on these topics in **Supplemental Text Section 1**.

1.1. Kīlauea Volcano

Kīlauea (**Figure 1**) is the youngest subaerial volcano produced by the Hawaiian hot spot. Kīlauea comprises a basaltic shield indented by a summit caldera, an East Rift Zone (ERZ), and a Southwest Rift Zone (SWRZ). Magma is supplied to the volcano from an inferred upwelling mantle plume (Wolfe et al. 2009) and moves sublaterally from the summit storage system into the rift zones. In the half-century before 2018, most of Kīlauea's eruptions occurred along the ERZ. It is thought that the ERZ consists of a semicontinuous largely molten core at ~3–5+ km depth overlain by solidified dikes, lava flows, and subordinate pyroclastic debris, and underlain by an olivine-rich crystal mush with low (<5%) melt fraction and a ductile rheology (e.g., Ryan 1988, Clague & Denlinger 1994, Johnson 1995). A weak, subhorizontal basal detachment fault (décollement) at a depth of ~8 km below sea level, dipping slightly landward, separates the volcanic edifice from the underlying Cretaceous seafloor (Hill & Zucca 1987). Gravitational

near-vertical planar zone that accommodates extension of a volcand

Rift zone:

extension of a volcano and facilitates lateral magma transport to its flanks

Caldera: large-scale volcanic depression caused by downdrop of fault-bounded blocks associated with evacuation of underlying magma

East Rift Zone (ERZ): Kīlauea's rift zone structure to the east of the summit (~125 km long including its submarine portion)

Dike: used herein to refer to a steeply dipping planar magma body

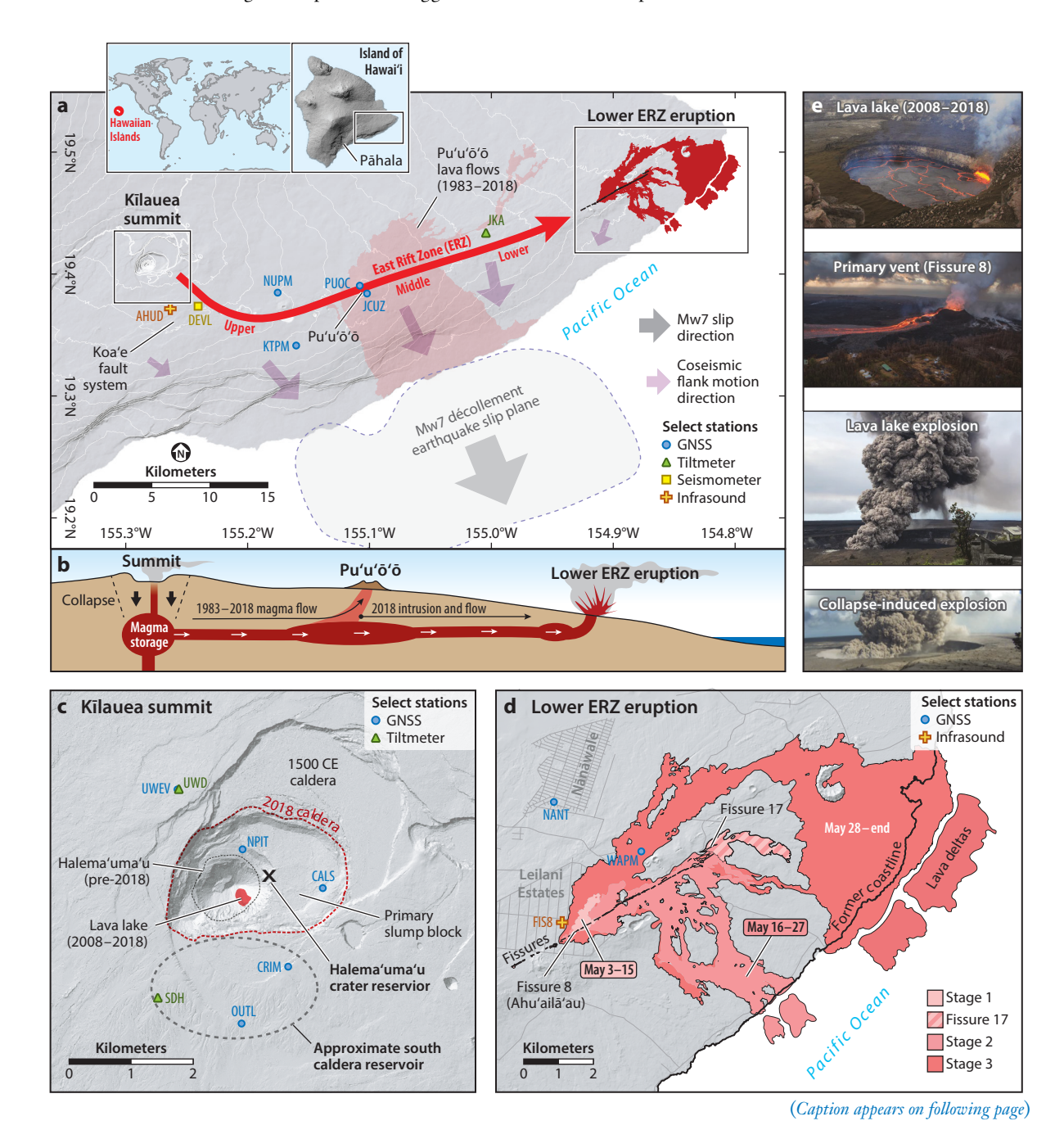
Olivine: the dominant mineral phase in most Hawaiian lavas, (Mg,Fe)₂SiO₄

1.2 Anderson et al.



stress on the edifice and intrusions of magma in the rift zones and summit facilitate slip on the décollement, which is resisted by frictional stresses (Denlinger & Flinders 2022). As a result, the south flank of the volcano, seaward of the rift zones, is mobile (Denlinger & Morgan 2014).

Kīlauea is renowned for effusive lava eruptions, but summit collapses and explosive activity are also common. Geologic interpretations suggest a summit-wide collapse at ca. 200 BCE and



www.annualreviews.org • The 2018 Kīlauea Eruption



Figure 1 (Figure appears on preceding page)

Eruption maps and photos, with selected monitoring stations (cf. Shiro et al. 2021). (a) Kīlauea Volcano with schematic magma flow path from summit to vent. The approximate slip plane of the ~Mw7 décollement earthquake is shown [some studies also favor a component of onshore rupture (Kehoe et al. 2019)]; purple arrows show approximate coseismic flank slip directions at a different scale. Three- and four-letter codes (e.g., NUPM) indicate monitoring stations. (b) Schematic cross section of panel a. Panels a and b adapted from Anderson et al. (2019) (US Geological Survey; public domain). (c) Summit, showing post-2018 topography. The approximate centroid of the HCR is noted with an "X," and the approximate region of the SCR is noted with a dashed line, which should not be interpreted as representing reservoir geometry or size. (d) Lower ERZ eruption with lava flows and deltas (Zoeller et al. 2020, Soule et al. 2021). (e) US Geological Survey eruption photographs (public domain). Abbreviations: ERZ, East Rift Zone; GNSS, Global Navigation Satellite System; HCR, Halema'uma'u crater reservoir; SCR, south caldera reservoir.

Lower ERZ (LERZ): portion of the East Rift Zone beyond 30 km downrift

Halema'uma'u crater reservoir (HCR): the shallow summit magma storage reservoir, thought to be centered at ~1-2 km depth; also referred to as the subcaldera reservoir

South caldera reservoir (SCR): the deeper crustal summit magma storage system, estimated at 3–6 km depth

Middle ERZ (MERZ): portion of the East Rift Zone from ~8 to ~30 km downrift

Slow slip event (SSE): temporary (usually minutes- to days-long) acceleration of slip of a fault plane that is much slower than an earthquake but faster than the generally continuous rate of background fault creep

Fissure: an elongate fracture or crack from which lava erupts, typically fed by a dike

another at ca. 1500 CE that created the modern caldera (Holcomb 1987, Swanson et al. 2014). Both of these collapses took place soon after the eruption of large basaltic flow fields, and both were followed by periods of dominantly explosive volcanism—the first lasting ~1,200 years and the second >300 years (Swanson et al. 2014). The modern caldera has been modified by smaller cycles of refilling and collapse, particularly in the nineteenth century, believed to be triggered by magma flow to the rift zones (**Supplemental Text Section 2**). Before 2018, the most recent lower ERZ (LERZ) intrusions and eruptions occurred in 1955 (88-day eruption) and 1960 (36-day eruption), both erupting on the order of 100 million cubic meters. Neither, however, led to large-scale summit collapse.

Modern monitoring data suggest the presence of two primary magma storage reservoirs at the summit: one centered at ~1–2 km depth in the southwestern sector of the 1500 CE caldera near Halema'uma'u crater [the Halema'uma'u crater reservoir (HCR); also referred to herein as the subcaldera reservoir] and a deeper, less well-characterized reservoir to the south [the south caldera reservoir (SCR)] (e.g., Poland et al. 2014). The relation between the reservoirs is ambiguous, and changes in their internal pressures appear to be correlated and anticorrelated over different time periods (e.g., Poland et al. 2021b, Crozier & Karlstrom 2022). Discrete magma storage zones also exist at shallow depth along the ERZ (~3 km or less)—typically thought to be residual from previous intrusions—and magma storage may also occur significantly in the deep rift below its molten core (e.g., Wright & Fiske 1971, Delaney et al. 1990, Wright & Klein 2014).

From 1983 to 2018, summit-supplied magma erupted semicontinuously from vents at or near Puʻuʻōʻō in the middle ERZ (MERZ), 20 km from the summit, fed by magma that first passed through the summit system (Heliker & Mattox 2003, Garcia et al. 2021). The near-rift portion of the décollement creeped (slipped) aseismically at a steady \sim 25 cm/year (Chen et al. 2019), punctuated by periodic slow slip events (SSEs) (Montgomery-Brown et al. 2015). At the summit, a lava lake formed in a new crater in Halemaʻumaʻu in 2008 and grew through the onset of the 2018 eruption to an area of 50,000 m² (Patrick et al. 2021). The lake was fed directly by the HCR, and variations in magma pressure caused changes in its height as well as flow activity near Puʻuʻōʻō, permitting the lake to be used as a reservoir pressure gauge (e.g., Anderson et al. 2015, Patrick et al. 2019b). Kīlauea's 2018 eruption was therefore staged in the dynamic context of a well-connected summit and rift system that had been active for decades.

1.2. A Brief Summary of the 2018 Eruption

On April 30, 2018 [day 0; Stage 1; **Figure 2**; all times are Hawaiian Standard Time (HST)], a fissure opened on the flank of Puʻuʻōʻō, and the floor of the cone collapsed as magma began flowing rapidly downrift into the LERZ (Neal et al. 2019, Poland et al. 2021a). On May 3 (day 3), lava began erupting in the Leilani Estates subdivision 20 km downrift of Puʻuʻōʻō and 40 km from the summit. The next day, a moment magnitude (Mw) \sim 7 earthquake—the largest on the island in 43 years—occurred on Kīlauea's basal décollement.

1.4 Anderson et al.



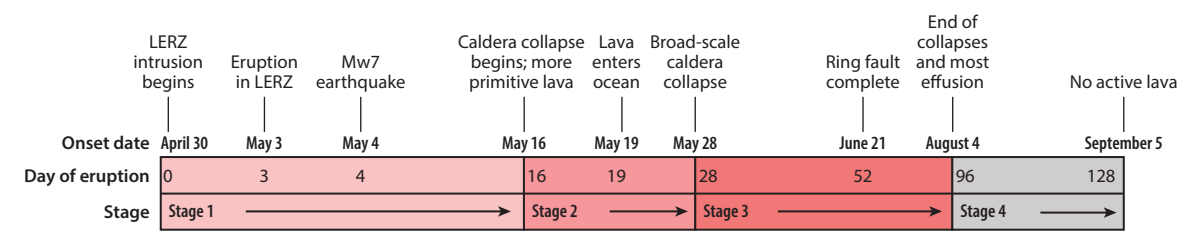


Figure 2

Primary eruption stages. Stage 1 (April 30 to May 15): LERZ intrusion, viscous lava flows, and pre-collapse summit drainage. Stage 2 (May 16 to 27): small-scale caldera collapse and increasing flow activity; more primitive lavas. Stage 3 (May 28 to August 3): high-rate collapse and eruption. Stage 4 (August 4 to September 5): post-collapse and minor lava effusion. Eruption day computed relative to April 30 (day 0). A number of chronologies have previously been proposed; this one aligns closely with Gansecki et al. (2019) but is modified slightly to capture major changes approximately concurrent in the summit and ERZ. Abbreviations: ERZ, East Rift Zone; LERZ, lower East Rift Zone.

Over the next two weeks, as the intrusion continued to widen and lengthen, a series of 24 fissures opened in the LERZ, producing lava fountains and small flows. Consequent evacuation of magma from the summit led to ground subsidence and cracking, withdrawal of the lava lake, and in mid-May (Stage 2) the onset of episodic (quasi-periodic) step-like caldera collapse, which triggered ejection of ash and ballistics from the vent. In the LERZ, more vigorous and destructive flows reached the ocean during this time. In late May (Stage 3) the surface expression of summit collapse began to broaden and the LERZ eruption focused at fissure 8 (which ultimately produced the Ahuʻailāʻau tephra cone). Through June and July, lava flows from fissure 8 destroyed several subdivisions, and the summit caldera grew to a volume of \sim 0.83 km³ and maximum depth of >500 m. Caldera collapse and most LERZ lava effusion ended abruptly in early August (days 94–96), although sporadic, weak venting of gas and lava continued for another month (Stage 4). Neal et al. (2019) presented a summary of these events.

The 2018 eruption was documented using in situ monitoring networks, remote-sensing platforms, and intensive field investigations, including the extensive use of unoccupied aircraft systems and rapid (daily) field sampling and chemical analyses of erupted lavas (e.g., Gansecki et al. 2019, Lundgren et al. 2019, Neal et al. 2019, James et al. 2020, Shiro et al. 2021). Selected eruption photos are shown in **Supplemental Figures 1–3**.

2. OBSERVATIONS AND MAIN FINDINGS

The diversity of observations and their high spatial and temporal density have served as the foundation for a wealth of studies, which we summarize in this section.

2.1. An Eruption Decades in the Making

Globally, the processes leading to large volcanic eruptions have rarely been documented, but Kīlauea's dense monitoring network offers a rare opportunity to assess the factors contributing to the 2018 eruption (Patrick et al. 2020). In this section we address the mechanism(s) that allowed stored magma to begin moving at high rates downrift into the LERZ for the first time in nearly 60 years, triggering the eruption. In later sections we address the question of why the eruption was so large.

The most important factor contributing to the 2018 eruption may have been long-term priming of the ERZ. Gravity-driven slip of Kīlauea's south flank along the décollement (Denlinger & Flinders 2022) gradually builds tensional stress across the rift zone, reducing the magma pressure

Magma supply rate (MSR): the rate at which magma is supplied to Kīlauea

required for downrift intrusions. Over the four decades preceding 2018, quasi-steady seaward flank motion at Kīlauea led to periodic intrusions in the upper and middle ERZ that occurred after the accumulation of ~1–5 MPa of across-rift tensional stress (Montgomery-Brown & Miklius 2020). In the LERZ, décollement slip rates are lower and intrusions less frequent, but similar tension may have accumulated between the most recent 1955/1960 intrusions and 2018 (Montgomery-Brown & Miklius 2020).

Other factors may also have served to weaken the rift zone, including magma storage in the MERZ associated with the sustained Puʻuʻōʻō eruption, moderate décollement earthquakes, and long-term magma leakage into the LERZ (Flinders et al. 2020a, Patrick et al. 2020, Pietruszka et al. 2021). Farquharson & Amelung (2020) also argued that extreme rainfall in 2018 increased pore pressure and weakened host rock, but interpretations of rainfall data have been controversial, and the resulting stress changes near Puʻuʻōʻō would have been very small compared to those induced by magma pressure changes (Poland et al. 2022, Mourey et al. 2023a).

Increasing magma pressure also provided more force to drive intrusions. Pressure in the summit reservoirs had gradually increased for years and was likely at its highest level in two decades (pressure in the SCR had particularly increased during the five years preceding the eruption) (Patrick et al. 2020, Crozier & Karlstrom 2022, Poland et al. 2022) (**Figure 3a**). After late 2017, earthquake fault orientations indicated changing stresses in the summit and ERZ (Lin & Shearer 2021). Pressurization accelerated in March 2018 and again in mid-April: Lava lakes at Pu'u'ō'ō and the summit rose by tens of meters (Neal et al. 2019, Patrick et al. 2020, Poland et al. 2022), earthquake rates increased (Cui et al. 2021), and seismic velocities—indicative of rock stressing and damage—underwent spatiotemporally complex changes (e.g., Olivier et al. 2019, Feng et al. 2020, Flinders et al. 2020a, Lin & Shearer 2021) (**Figure 3b**). Nonetheless, large shallow magma pressures were precluded by the open lava lake vents at the summit and Pu'u'ō'ō (Anderson et al. 2019).

The cause of pre-eruptive pressurization remains uncertain, and more than one process may have played a role. During Kīlauea's Pu'u'ō'ō eruption, changes in magma pressure were caused by imbalances between magma supply rate (MSR) and eruption rate (Patrick et al. 2019a). An increase in MSR may be suggested by higher rates of lower-mid crustal earthquakes after late 2017 (Flinders et al. 2020a, Patrick et al. 2020, Cui et al. 2021) and higher rates of mantle earthquakes southwest of Kīlauea (Pāhala region) after 2015 (Burgess & Roman 2021). Influxes of primitive melt may also be suggested by high ³He/⁴He ratios observed in the LERZ eight months before the eruption (McMurtry et al. 2019) and the presence of primitive olivine in 2018-erupted lava (Gansecki et al. 2019; Mourey et al. 2023a,b). However, the relation between these observations and MSR remains ambiguous, and some models of geophysical data do not indicate unusual changes in shallow magma temperature or volatile content in the months preceding the eruption (Crozier & Karlstrom 2022). More directly, waning lava effusion and MERZ SO₂ emission rates in early 2018 (Kern et al. 2020) suggest a backup in the magma system near Pu'u'ō'ō, as had preceded some previous ERZ intrusions at Kīlauea (Orr et al. 2015, Patrick et al. 2019a). The backup may have been caused by a restriction in the eruptive conduit (Patrick et al. 2020), with an increase in magma density and viscosity in the ERZ related to degassing through the summit lava lake as a possible contributing factor (Lerner et al. 2021).

2.2. Rift Zone Intrusion and Eruption

2.2.1. Intrusion and décollement earthquake. Kīlauea's rift zone magmatic-tectonic system is tightly coupled (**Figure 4**). Injection of magma into the ERZ can promote décollement slip manifested by large, damaging earthquakes [e.g., the 1975 Mw7.7 event (Ando 1979)] or smaller SSEs (Montgomery-Brown et al. 2015), while décollement slip promotes both the initiation and

1.6 Anderson et al.



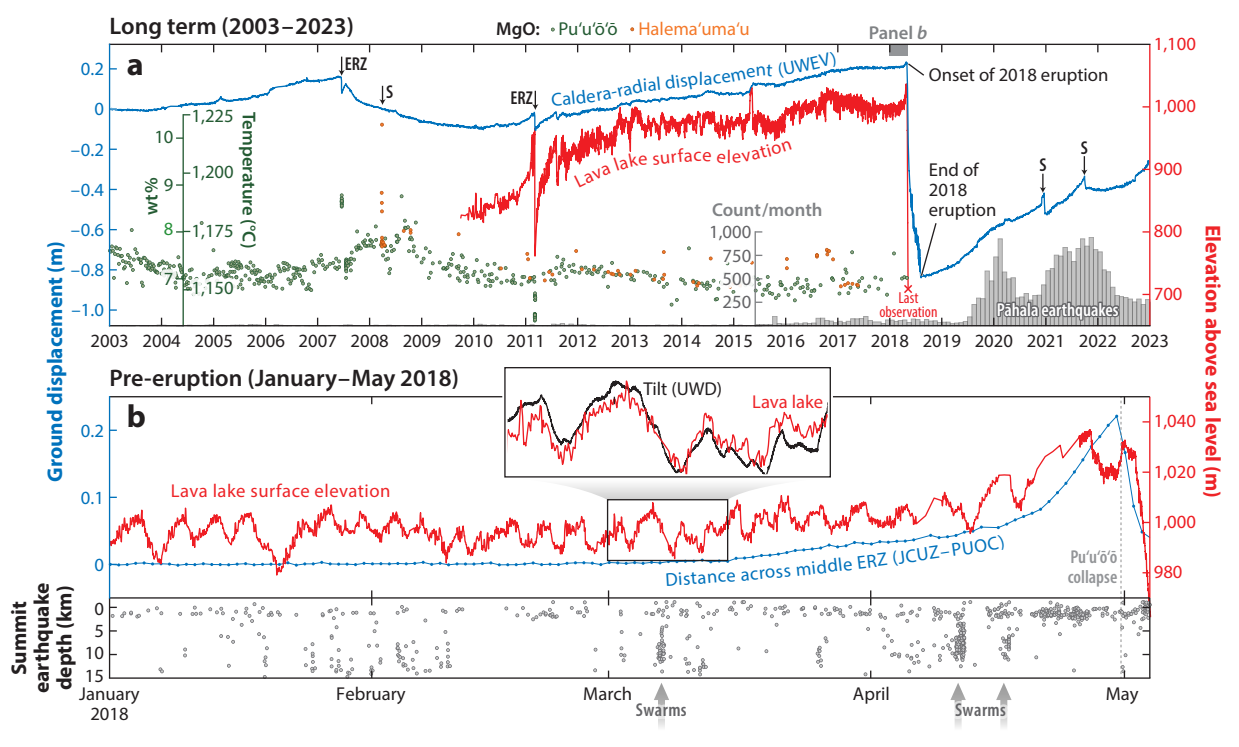


Figure 3

(a) Twenty years of data spanning the eruption. Shown are caldera-radial GNSS ground displacements, 2009–2018 summit lava lake elevation from Patrick et al. (2019d) ("X" denotes last observation), bulk rock MgO through May 1, 2018 [some outliers excluded (R.L. Lee et al. data release in progress) with temperatures computed using relations in Helz & Thornber (1987), and M > 1.5 Hawaiian Volcano Observatory catalog earthquakes in the Pāhala region at >25 km depth. Arrows denoted "ERZ" and "S" indicate ERZ intrusions and/or eruptions and summit eruption onsets, respectively (excluding 2018). Correlation between GNSS and lake surface elevation over this long period is affected by other magma reservoirs and possibly long-term changes in lava density (Patrick et al. 2019b, Crozier & Karlstrom 2022). After 2012, MgO remained largely steady as a balance between supply of new magma to the summit reservoirs and output of cooling magma to the ERZ was broadly attained. (b) Approximately 4 months preceding the eruption. (Top) Summit lava lake elevation and GNSS-measured distance across the ERZ at Pu'u'ō'ō. Variations in lava lake elevation were caused chiefly by pressure cycles in the HCR (Anderson et al. 2015), as shown in the inset, which compares lava lake elevation to ground tilt at station UWD. (Bottom) M > 1 summit earthquakes, with notable swarms denoted by gray gradient arrows. UWEV, JCUZ, and PUOC are monitoring station names (see Figure 1). Abbreviations: ERZ, East Rift Zone; GNSS, Global Navigation Satellite System; HCR, Halema'uma'u crater reservoir.

growth of rift zone intrusions (Montgomery-Brown et al. 2015). The complex interplay between gravitational, magmatic, and frictional forces revealed during and after the 2018 eruption yields new insights into these closely coupled physical processes that govern much of Kīlauea's activity (Supplemental Text Section 3).

The LERZ intrusion began with the collapse of Pu'u'ō'ō and was indicated by downrift propagation of earthquake hypocenters at a velocity that decreased over 1-2 days before stalling at a distance of ~20 km (Lengliné et al. 2021, Townsend & Huang 2022), accompanied by as much as ~30 cm of MERZ subsidence near Pu'u'ō'ō (Figures 5 and 6; Supplemental Figure 4). MERZ volume loss extended both uprift and downrift of Pu'u'ō'ō and continued at a decaying rate throughout the eruption; models suggest a volume loss of $\sim 0.05 \text{ km}^3$ by day 17 (Neal et al. 2019) (subsurface volume changes are summarized in Supplemental Text Section 5). Downrift, the LERZ extended, but the summit did not begin to subside significantly until $\sim 2-3$ days after the

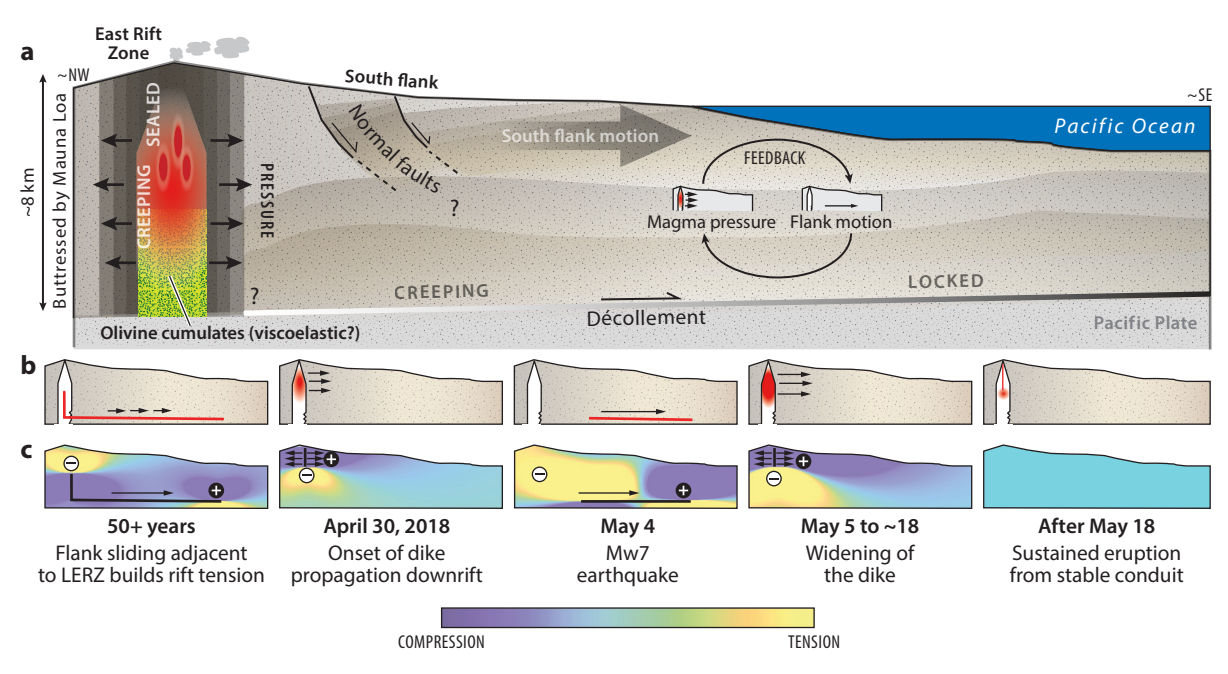


Figure 4

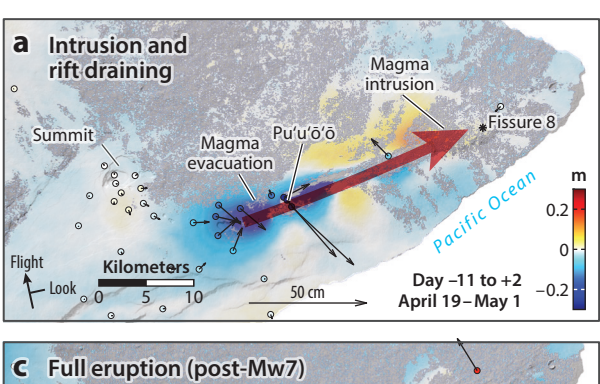
Schematic cross section of the ERZ (not to scale). (a) Coupling between the seaward-sliding flank and the rift zone magma system sets up a feedback process encouraging cycles of décollement slip and magma intrusion. Panel a adapted from Montgomery-Brown et al. (2015) (US Geological Survey; public domain). (b,c) Magmatic-tectonic processes before and during the 2018 eruption showing slip and magma pressure (b) and rift-normal stresses (c), demonstrating how rift opening and flank sliding processes encourage one another. The absolute scales on these models vary significantly, so only general senses of compression or tension are presented. Abbreviations: ERZ, East Rift Zone; LERZ, lower East Rift Zone.

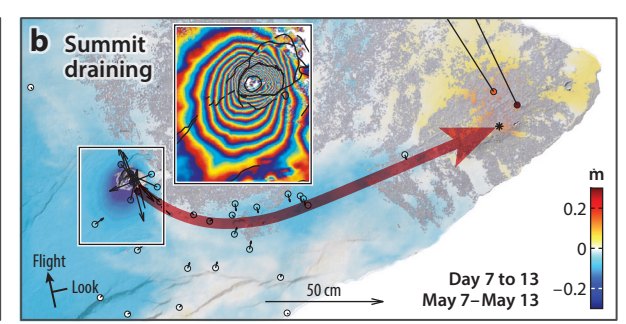
> collapse of Pu'u'ō'ō. These observations accord with downrift (and possibly downward) growth of a dike-like (tabular) intrusion fed by a shallow depressurizing magma storage zone near Pu'u'ō'ō (Chen et al. 2019, Neal et al. 2019, Kundu et al. 2020, Lengliné et al. 2021) and only later supplied at high rate from the summit (Townsend & Huang 2022). The intrusion propagated several kilometers farther downrift on days 9-10, feeding new fissures (Neal et al. 2019), and continued opening rapidly through day 18. After this time, greatly reduced rates of deformation and earthquakes in the LERZ indicated a stable, open conduit system. Downrift magma transport likely occurred somewhere between ~2 and 4 km depth, as suggested by preliminary models of geodetic data as well as CO₂ recorded in a relatively undegassed pumice sample (Neal et al. 2019, Lerner et al. 2021). The LERZ intrusion volume was $\sim 0.1 \text{ km}^3$, and its maximum opening was of order 4 m (Neal et al. 2019).

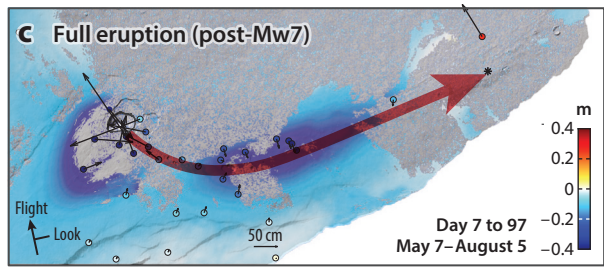
> At 12:32 PM on May 4, following the first phase of downrift magma propagation, the 2018 ~Mw7 earthquake struck. Seismic, geodetic, and tsunami data suggest as much as 2-3+ m of lowangle thrust faulting mostly at a low rupture speed of $\sim 1-2$ km/s (consistent with weak, altered sediments at the basal décollement) at \sim 5-8+ km depth along the décollement, perpendicular to shore, in an arcuate pattern offshore of the south flank (Figure 1) in a similar location as an Mw7.7 earthquake in 1975 (Bai et al. 2018, Lay et al. 2018, Liu et al. 2018, Chen et al. 2019, Kehoe et al. 2019, Neal et al. 2019, Kundu et al. 2020, Lin et al. 2020, Wei et al. 2022). Portions of Kīlauea's subaerial south flank moved as much as 0.7 m seaward (Neal et al. 2019). The coseismic rupture patch likely extended into a region of the décollement that hosts SSEs, indicating that

1.8 Anderson et al.









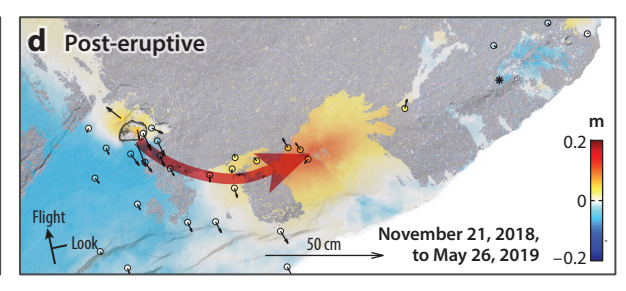


Figure 5

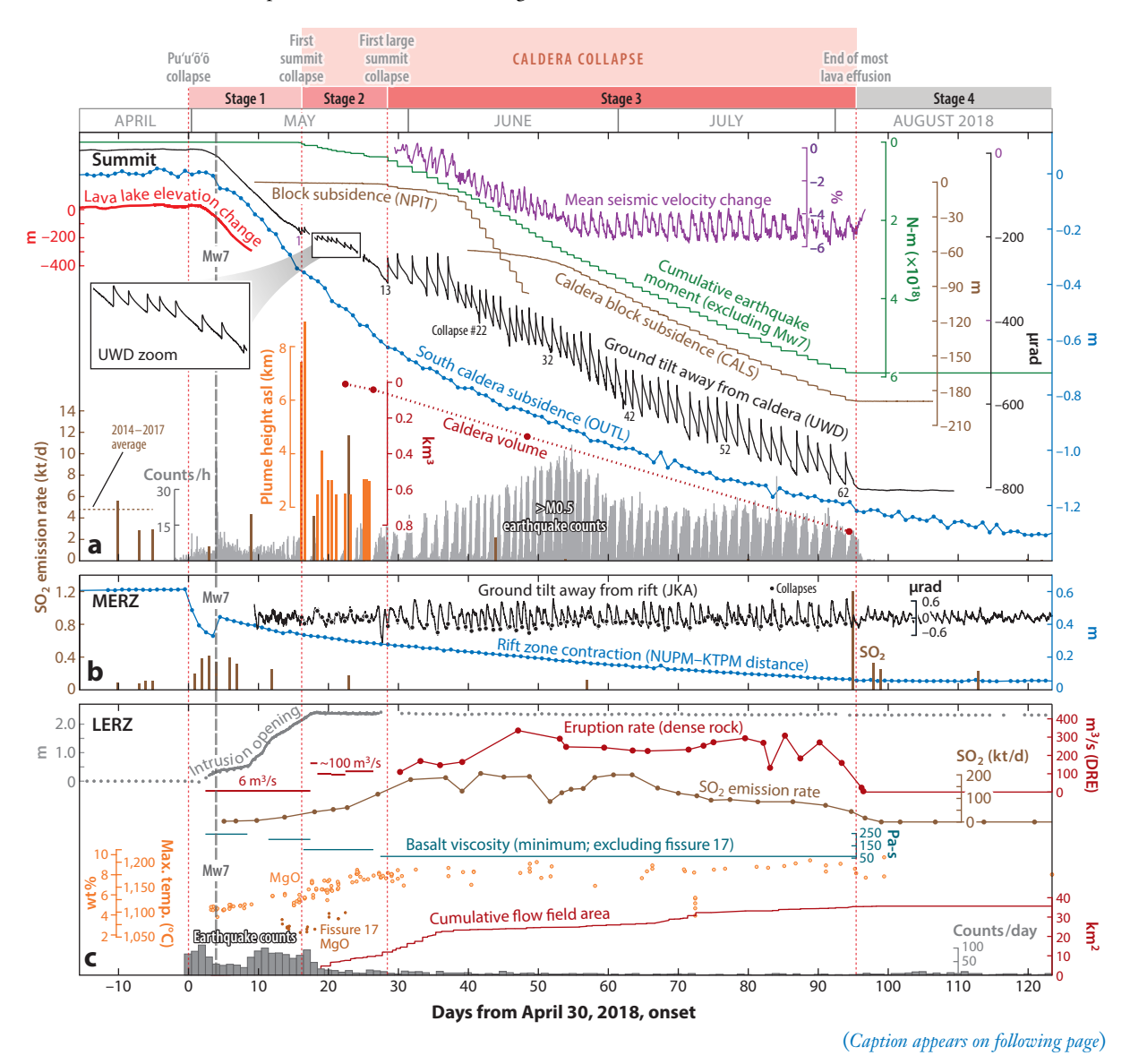
InSAR images showing total distance changes between the ground and an orbiting Sentinel-1 satellite, recorded at an oblique angle (34°). The color scale differs between panels; gray indicates no data. Black vectors and filled circles indicate horizontal GNSS displacements and GNSS displacements projected into the satellite line of sight, respectively. Large red arrows denote a conceptual primary magma flow path. (a) Withdrawal of magma from the MERZ to the LERZ before the onset of summit subsidence during the first two days of the eruption (relatively minor pre-eruptive deformation is also included). (b) Days 7-13, showing rapid draining of the summit and continued inflation of the LERZ (shown in more detail in Neal et al. 2019). The inset shows rewrapped data from Anderson et al. (2019); each color fringe represents 2.8 cm of ground motion. (c) Days 7-97, showing subsidence of the summit and MERZ. Maximum summit subsidence of >1 m and >500 m inside and outside of the new caldera, respectively, is obscured due to decorrelation and unwrapping challenges; see Supplemental Figure 5. LERZ deformations are not visible due to decorrelation. (d) The post-eruptive period, showing inflation of the MERZ and simultaneous subsidence and uplift in different parts of the summit region. Abbreviations: GNSS, Global Navigation Satellite System; InSAR, interferometric synthetic aperture radar; LERZ, lower East Rift Zone; MERZ, middle East Rift Zone.

fault sections may slip with diverse behaviors (Supplemental Figure 6) (Kehoe et al. 2019, Lin et al. 2020). The US Geological Survey (USGS) and Global Centroid Moment Tensor Project used broadband seismic data to infer thrust faulting on a ~20 degree-dipping fault plane with a magnitude of Mw6.9 (Neal et al. 2019), but other studies that also use geodetic and tsunami data suggest shallower dip angles of 2.5-7.5 degrees—more consistent with the décollement (Hill & Zucca 1987)—and preferred magnitudes ranging from 7.1 to 7.2 (e.g., Bai et al. 2018, Lay et al. 2018, Chen et al. 2019, Lin et al. 2020). Splay fault activation may explain some of the variation in estimated dip angles and also an observed 40-cm tsunami (Bai et al. 2018, Lin et al. 2020). In this review we refer to the event as ~Mw7 but consider this value approximate.

The earthquake resulted from several related processes. In the years before 2018, long-term slip on the creeping portion of the décollement—with possible contribution from stresses imparted by increased magma storage in the summit and rift—gradually increased Coulomb stress on its locked portion (Chen et al. 2019, Kundu et al. 2020) (Figure 4b). In 2018, rapid migration of magma from the MERZ to the LERZ further stressed the décollement, finally triggering the earthquake (Chen et al. 2019, Kundu et al. 2020). The earthquake released 20-35 years of accumulated stress inadequate to account for the entire period from the 1975 Mw7.7 earthquake (Chen et al. 2019).

Observations are consistent with ideas that only small stress changes are required for bi-directional triggering between flank slip and rift intrusions (Montgomery-Brown et al. 2015).

GNSS: Global Navigation Satellite System The earthquake produced tensile stress changes of as much as 0.4 MPa in the rift system (Kundu et al. 2020), which may have aided magma transport downrift (Neal et al. 2019)—possibly explaining, in part, increases in rates of ground deformation and lava lake withdrawal at the summit around the time of the \sim Mw7 earthquake (Anderson et al. 2019). Reduction of magma pressure during the eruption, in turn, reversed secular (long-term) southward motion of south flank Global Navigation Satellite System (GNSS) stations, while gravitational forces continued to move the flank eastward (Denlinger & Flinders 2022). Observations are consistent with slip on a weak décollement driven by both magmatic and gravitational forces, and a hot viscoelastic deeper rift below 2 km (Denlinger & Flinders 2022).



1.10 Anderson et al.



Figure 6 (Figure appears on preceding page)

ARjats.cls

Select co-eruptive time series. (a) Summit, showing seismic velocity change, cumulative seismic moment, subsidence of caldera blocks in high-rate GNSS data, cyclic ground deformation recorded outside the caldera [tiltmeter UWD; long-term tilt is not representative of all stations (Anderson & Johanson 2022)], gradual subsidence in the south caldera region, tephra plume heights during May, caldera volume, SO₂ emissions, and hourly earthquake counts. (b) MERZ, showing ground tilt cycles at station JKA (highpass-filtered; black dots indicate summit collapse times), long-term rift contraction (offset on May 4 caused by ~Mw7 earthquake), and SO₂ emissions, which are poorly characterized for most of July (the large value in early August is also not well understood). (c) LERZ, showing intrusion (dike) opening on the north channels of two GNSS stations (WAPM through day 29 and then NANT; dots are daily solutions, and dense points are high-rate solutions), eruption rate (bars are time averages), SO2 emissions, the viscosity and geochemistry of erupted lava (cf. Gansecki et al. 2019), flow field area, and daily earthquake counts. Values of MgO are derived from bulk rock ED-XRF and WD-XRF, and temperatures represent an upper bound. Data are from Elias et al. (2018), Gansecki et al. (2019), Lundgren et al. (2019), Patrick et al. (2019d), Shelly & Thelen (2019), Kern et al. (2020), Soldati et al. (2021), Hotovec-Ellis et al. (2022), Hawaiian Volcano Observatory earthquake catalog, and NOAA NEXRAD (https://www.ncdc.noaa.gov/nexradinv/) with processing by Ryan Cahalan as in Cahalan et al. (2023). For uncertainties in data, see the source publications. Three- and four-letter codes (e.g., CALS) indicate monitoring station names (see Figure 1). Abbreviations: ED-XRF, energy dispersive x-ray fluorescence; GNSS, Global Navigation Satellite System; LERZ, lower East Rift Zone; MERZ, middle East Rift Zone; WD-XRF, wavelength dispersive x-ray fluorescence.

2.2.2. Fissures, fountains, and lava flows. A century-long study of Hawaiian eruptions has been fundamental to volcanologists' understanding of fissures and lava flows worldwide (Cashman & Mangan 2014). Intensive monitoring of the 2018 eruption adds importantly to this body of knowledge and sheds new light on the volcano's interconnected summit-rift magma system.

Lavas erupted in 2018 varied systematically in composition and over a wider range (bulk rock MgO = 2.5-8.5 wt%) than most previous Kīlauea eruptions (**Figures 6c** and **7**). The first flows erupted (Stage 1; <1 vol% of 2018 flows) were composed of cool, highly evolved, high-Ti basalt with low-Fo olivine (4-5 wt% MgO; <Fo₈₀; ~1,100°C) and were some of the most evolved to have erupted in recent centuries at Kīlauea (Gansecki et al. 2019). Late Stage 1 lava flows were less evolved (~6 wt% MgO) and transitional between early Stage 1 and Stage 2. Stage 2 lava flows (3–7 vol% of 2018 flows) were more mafic and hotter (7–8 wt% MgO; \sim 1,130°C), while during Stage 3 (>92 vol% of 2018 lavas), bulk magma compositions, phenocryst assemblages, and temperatures stabilized at values (7-9 wt% MgO; 1,150°C) only slightly higher than those of recent lava erupted at the summit and Pu'u'ō'ō (Gansecki et al. 2019, Pietruszka et al. 2021). The compositional evolution follows patterns of LERZ eruptive sequences in 1840, 1955, and 1960 (e.g., Wright & Fiske 1971, Helz & Wright 1992, Wright & Helz 1996) and appears to have been caused by the early eruption of LERZ-stored (and possibly some MERZ-stored) magmas that had undergone differentiation and were subsequently flushed and/or bypassed by more primitive magma from uprift (Gansecki et al. 2019, Lerner et al. 2021, Wieser et al. 2021, Mourey et al. 2022, Wieser et al. 2022).

In concert with compositional variations, the viscosities of erupted lava varied by more than three orders of magnitude (Roman et al. 2021, Soldati et al. 2021), exerting an important control on eruption rate, dynamics, and hazard. The transition to more primitive and less viscous lava was associated with increased effusion rates, faster-moving and farther-reaching flows, and the cessation of mild Stage 1 explosive activity (Gansecki et al. 2019, Dietterich et al. 2021, Soldati et al. 2021, Wieser et al. 2021). Particularly notable was the eruption of andesitic/icelanditic bulk composition lava (2.5-4 wt% MgO; ~1030-1080°C) from portions of fissure 17, including episodic Strombolian-like explosions likely caused in part by the high viscosity and water content (~2 wt%) of erupting lava (Dietterich et al. 2021, Soldati et al. 2021, Thelen et al. 2022, Wieser et al. 2022). Roman et al. (2021) also argued that changes in magma viscosity during 2018 caused variations in rift-perpendicular stresses and rotations in earthquake fault planes, suggesting a novel future monitoring technique.

Bulk rock: the composition of erupted material determined by physically crushing and homogenizing glass and minerals before analysis

MgO: measure of the magnesium content of glass or whole rock, which can be used to track magma differentiation (lower Mg = moredifferentiated) and to infer eruptive temperatures

Evolved magma: a magma that has undergone extensive differentiation (usually MgO < 6.5 wt%), often found in rift zones at Kīlauea



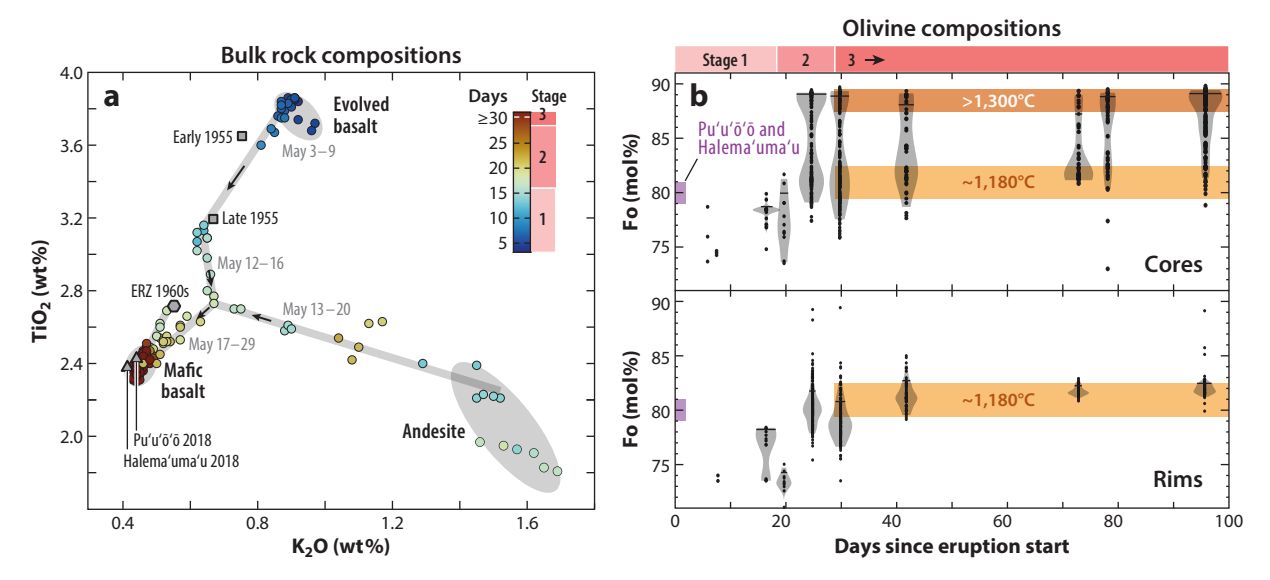


Figure 7

Geochemical characteristics of LERZ eruption products. (a) Bulk rock TiO₂ versus K₂O, distinguishing magmas that have fractionated Fe-Ti oxides (andesite) from those that did not (mafic and evolved basalts), illustrating the evolution of magma mixing between the three main end members involved in the eruption. Colors (with trends indicated by black arrows) show changes in magma composition during the first month; gray symbols show compositions from recent historical eruptions. Panel a adapted from Gansecki et al. (2019); reprinted with permission from AAAS. (b) Olivine core (top) and rim (bottom) forsterite compositional evolution as a proxy for magma differentiation. Data are from Gansecki et al. (2019), Lerner et al. (2021), Wieser et al. (2021), and Mourey et al. (2022). Black dots show individual samples, gray-shaded regions (violins) show population statistics with truncation at 5% and 95% values, and black bars show kernel density estimates. Samples erupted within a few days of each other are grouped together into one population. Purple boxes show Pu'u'ō'ō and Halema'uma'u representative olivine compositions for comparison (Mourey et al. 2022). After ~3 weeks, LERZ olivine cores—which preserve information about their magma of origin—often show bimodal distributions with both a high Fo (>87 mol%) component thought to indicate summit magma. Olivine rims—which preserve information about their final host magma—clustered around the same range (80–82 mol%) after week 3, suggesting most crystals were forming rims at or near melt-olivine equilibrium with the large volume of summit-derived, mafic basalt. Temperatures are calculated from olivine compositions from Mourey et al. (2023a). Abbreviations: ERZ, East Rift Zone; LERZ, lower East Rift Zone.

Fo: forsterite; measure of the relative magnesium content of olivine [Fo = Mg/ (Mg + Fe) \times 100], in units of mol% (e.g., 88.5%) or mol fraction (e.g., 0.885); high-Fo olivine (e.g., >87%) forms in primitive magmas, whereas low-Fo olivine (e.g., <82%) forms in more evolved magmas

The eruption provided an unusual opportunity to closely observe the birth of a fissure eruption and a range of mildly explosive activity. Variations in Strombolian and Hawaiian eruptive style were governed by melt viscosity, mass flux, and coupling between exsolved volatiles and magma and were modulated at very shallow depths (<100 m) (Houghton et al. 2021, Walker et al. 2023). Throughout the eruption, fissure 8 produced ~30- to 80-m-high fountains in which adiabatic expansion of gas in the plume triggered secondary brittle fragmentation of clasts (Namiki et al. 2021). For most of Stage 3, these fountains supplied a stable lava channel with near-vent velocities at times exceeding 15 m/s, high Reynolds and Froude numbers flow, transitional turbulent behavior, and standing waves (e.g., Patrick et al. 2019c, Dietterich et al. 2022). The channel minimized flow-field expansion and efficiently transported lava over large distances [~85% of the bulk flow volume was emplaced > 8 km from the vent (Dietterich et al. 2021)], with most flow-field expansion occurring primarily on the distal coastal plain, where low slopes contributed to channel diversions and secondary extrusions along the flow margins. Observations highlight the importance of capturing effusion-rate variations for effective hazard forecasting and provide a natural laboratory for testing and developing lava flow fluid dynamical theory and propagation models (e.g., deGraffenried et al. 2021, Dietterich et al. 2022).

1.12 Anderson et al.



Effusion rates at fissure 8 varied cyclically in at least two ways. First, minute-scale pulsing activity may reflect a shallow gas-driven process or pressure oscillations in a deformable conduit (Patrick et al. 2019c, Piombo & Dragoni 2021). Second, summit caldera collapse events 40 km uprift were followed by surge-like pressure pulses in the ERZ (Patrick et al. 2019c), evident as ground deformation transients along the ERZ and, at the vent, rapid increases in effusion rate and seismic and infrasonic tremor amplitudes (Patrick et al. 2019c, Lyons et al. 2021, Thelen et al. 2022). Surges began at the vent within 20 min of summit collapses, but eruption rates continued to rise for ~2–4 h before gradually decaying (Patrick et al. 2019c, Lyons et al. 2021). Post-collapse changes in seismic velocities in the LERZ have been attributed to the surges as well as structural weakening of rock related to seismic shaking (Wu et al. 2020). Surges demonstrate that important changes in hazard and eruption style can be triggered by events tens of kilometers distant and also serve as unique impulse-response tests of the magma system (Section 3.2.1).

A total of 0.9-1.4 km³ of lava [dense-rock-equivalent (DRE)] was erupted in 2018 (Dietterich et al. 2021, Soule et al. 2021), representing roughly a decade's worth of average magma supply to the volcano. More than half was emplaced as submarine lava deltas, which in places exceed 200 m in thickness (Dietterich et al. 2021, Soule et al. 2021). The average fissure 8 eruption rate of 250 m³/s is two orders of magnitude higher than typical MSRs to Kīlauea, indicating that eruption dynamics were not governed by mantle supply [for comparison, average Pu'u'ō'ō eruption rates were $\sim 2-6$ m³/s (Orr et al. 2015)].

Prodigious gas emissions accompanied the LERZ eruption, with SO₂ emission rates exceeding 100 kt/day (Kern et al. 2020) [during 2014–2017 Kīlauea's average emission rates were 5.1 kt/day, mostly from the summit (Elias et al. 2018)]. LERZ CO₂/SO₂ ratios of ~0.3 are consistent with loss of relatively insoluble CO2 at the summit, and relatively soluble SO2 at the vent, as in prior years (Kern et al. 2020). The eruption produced 7–14 Mt of SO₂ (and 0.5–2.8 Mt CO₂), making it one of the largest volcanic SO₂ sources of the past two decades (Kern et al. 2020). Together with petrologic constraints on magmatic sulfur content (e.g., Lerner et al. 2021), SO₂ emissions imply the eruption of 1.1-2.3 km³ of lava (DRE, at 68% confidence), similar to but generally higher than estimates based on emplaced lava flow volumes (Kern et al. 2020, Dietterich et al. 2021).

2.3. Summit Eruption and Collapse

Magma evacuation from the summit toward the ERZ caused subsidence, withdrawal of the lava lake, ground cracking, and slip on faults in the Koa'e fault system south of the caldera (Wang et al. 2019). Step-like caldera collapse occurred around Halema'uma'u crater, while gradually declining ground subsidence was observed in the south caldera region (inferences for magma storage are discussed in Section 3.1).

2.3.1. Magma withdrawal and the onset of caldera collapse. During Stage 1, the summit subsided at up to ~10 cm/day and the lava lake drained in its vent at ~50 m/day (Anderson et al. 2019) (Figures 5 and 6a; Supplemental Figure 7). These observations offer unprecedented insight into shallow magma storage and the buildup to a caldera collapse.

Many of the insights into the 2018 eruption were derived from the summit lava lake and demonstrate the scientific value of instrumenting active lava lake systems around the world. The lake's volumetric draining rate varied as a function of vent geometry, but its surface fell at a nearly constant rate—reflecting static equilibrium between the lake and the HCR (Anderson et al. 2019, Patrick et al. 2019d). The rate of lake withdrawal implies that the reservoir was depressurizing at ~1.25 MPa/day, which (given reasonable initial reservoir pressure) was too high to be sustained for more than a few weeks. Thus, caldera collapse must have served to increase pressure in the reservoir and thereby sustain the months-long eruption (Anderson et al. 2019). Jointly modeling Magma differentiation: the process of chemical and mineralogical evolution of magmas as they crystallize

Primitive magma: magma that has undergone little differentiation, typically with a high MgO content (usually >12 wt%) and temperature

Reynolds number: the ratio of inertial to viscous forces in a fluid and a measure of the tendency of flow to be turbulent

Froude number: the ratio of inertial to gravitational forces in a fluid



Very long period (VLP): seismic waves with energy concentrated at periods above ~2 s

lava lake and geodetic data also offers a rare opportunity to resolve both the geometry and total volume of the HCR (Section 3.1).

As the lava lake drained, summit infrasonic and seismic tremor steadily increased (Soubestre et al. 2021, Thelen et al. 2022), and destabilized vent walls frequently collapsed, resulting in chaotic flow dynamics, spattering, and small explosions (Section 2.3.3). As occurred over the previous decade, rockfalls and other perturbations triggered multiple seismically detectable modes of magma resonance of the lake-conduit-reservoir system, which evolved as the lake drained and yielded insights into system properties and storage/transport geometries (Dawson & Chouet 2014, Liang & Dunham 2020, Crozier & Karlstrom 2021, Soubestre et al. 2021).

By day 9, the lake surface had fallen >300 m and vanished at the bottom of an empty, roughly cylindrical, 11.5-million-m³ vent. Vent geometry was captured in detail using structure-frommotion imagery (Patrick et al. 2019d) and, when combined with gravity changes recorded while the lake drained (some of the largest ever recorded at a volcano by continuous measurements), provided a rare opportunity to constrain the in situ density of a lava lake [\sim 1700 kg/m³ in its upper \sim 200 m (Poland et al. 2021a)]. Density was higher than over the previous decade, possibly due to gradual outgassing of summit magma (Poland et al. 2021a).

A major question in volcanology has long been the critical volume and pressure thresholds at which magma reservoirs fail and calderas begin to collapse. Anderson et al. (2019) combined lava lake and geodetic data to estimate that episodic reservoir failure began on day 16 after withdrawal of <4% of stored magma had reduced reservoir pressure by \sim 17 MPa and induced a shear stress of 8–13 MPa on ring faults [some small, early-stage fault slip may have begun sooner (**Supplemental Text Section 4.1**)]. These results suggest that calderas may begin to form after relatively little magma is withdrawn (Anderson et al. 2019).

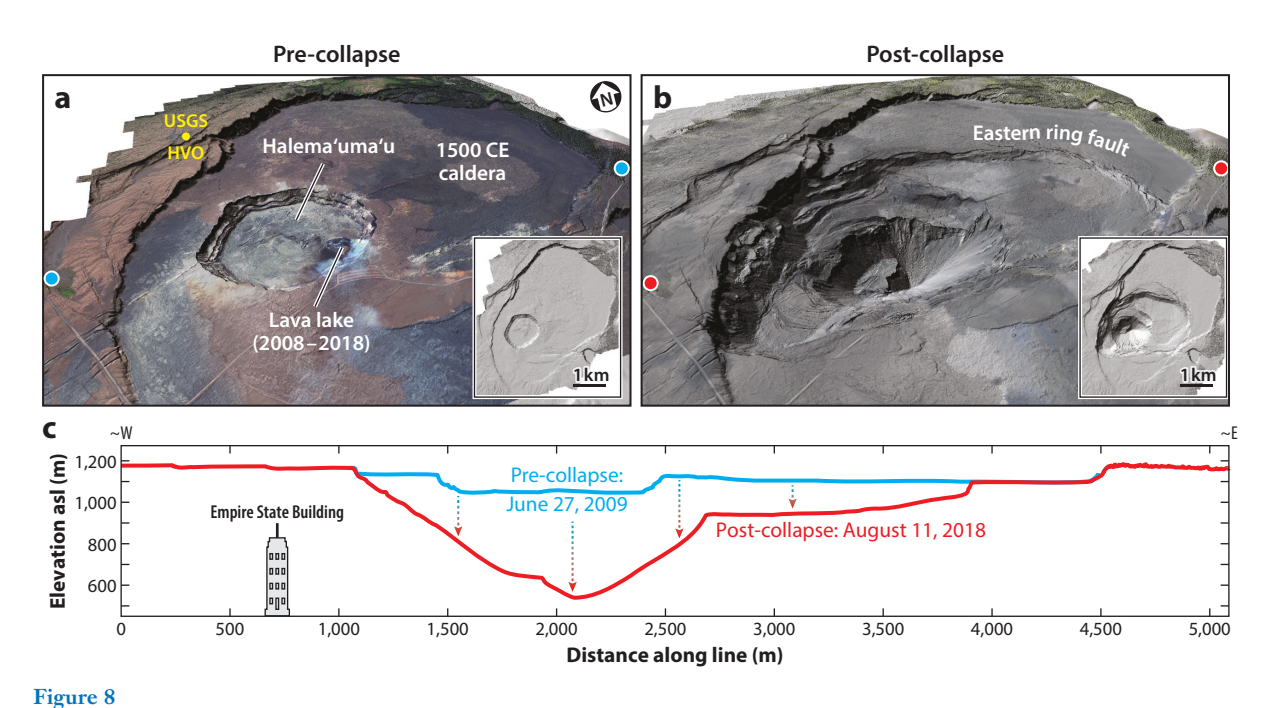
2.3.2. Mechanics and dynamics of caldera collapse. Collapse calderas form when large-scale magma evacuation causes foundering of reservoir roof rock, producing some of Earth's largest and most hazardous eruptions. Yet, only a handful of collapses have been observed historically—notably during basaltic eruptions at Fernandina, Miyakejima, Bárdarbunga, and Piton de la Fournaise volcanoes (e.g., Simkin & Howard 1970, Kumagai et al. 2001, Michon et al. 2009, Gudmundsson et al. 2016). Historical basaltic collapses appear to have been driven by lateral magma withdrawal, and geophysical data indicate that nearly all evolved episodically, but observations from most are limited and many of the governing physical processes have been poorly understood.

Kīlauea's 2018 caldera (**Figure 8**) grew through a series of 62 periodic approximately day-long cycles (mean recurrence interval of 1.3 d), each punctuated by abrupt seconds-long subsidence (collapse) of rock above the subcaldera magma reservoir (**Figures 6a** and **9**). The first 12 collapses (Stage 2 of the eruption) were associated with localized vent enlargement within Halema'uma'u crater (Anderson et al. 2019) and were coincident with abrupt, ramp-like, upward-and-outward centimeter-scale motion of the volcano's summit away from the vent over 10–30 s; atmospheric rarefactions attributable to ground subsidence within the growing vent (collapse pit) itself; radiation of very long period (VLP) seismic energy equivalent to ~Mw5 earthquakes (**Supplemental Figure 8**); and ejection of tephra (Neal et al. 2019, Flinders et al. 2020b, Tepp et al. 2020, Anderson & Johanson 2022, Thelen et al. 2022). Some similar but smaller geophysical signals were observed previously at Kīlauea's summit during the 2008–2018 lava lake era and in the days immediately preceding the onset of collapse (Lai et al. 2021, Poland et al. 2021b, Thelen et al. 2022).

Broad-scale surface collapse began with the thirteenth event (Stage 3) and subsequently proceeded in the form of meters-scale subsidence of semicoherent surface blocks surrounding a central rubbly collapse pit and separated by a growing network of faults and scarps. These changes

1.14 Anderson et al.





Rendered perspective views to the north-northeast across Kīlauea's summit (a) before collapse (2009) and (b) after collapse (August 11, 2018) derived from digital elevation models. Insets show vertical-perspective shaded relief maps. (c) East-west cross sections passing through blue dots (pre-collapse) and red dots (post-collapse), with New York's Empire State Building (440 m) for approximate scale.

Panel c adapted from Neal et al. (2019) (US Geological Survey; public domain). Abbreviation: USGS HVO, US Geological Survey Hawaiian Volcano Observatory.

were reflected in seismic velocity changes of >8% (Hotovec-Ellis et al. 2022). The seismic and

were reflected in seismic velocity changes of >8% (Hotovec-Ellis et al. 2022). The seismic and geodetic signature of Stage 3 collapses was markedly larger than during Stage 2, and included ground displacements of up to 20 cm outside of the caldera over <10 s, and increased high-frequency seismic shaking. Post-collapse deformation pulses and surges in eruption rate were observed during this time in the LERZ. Tephra emissions rapidly declined, but infrasound rarefactions continued. Between abrupt collapses, the ground around the caldera moved inward and downward at a slowing rate, but rates of caldera block subsidence and volcano-tectonic (VT) earthquakes increased together before often reaching a steady state (Tepp et al. 2020, Anderson & Johanson 2022, Wang et al. 2023) (Figure 9).

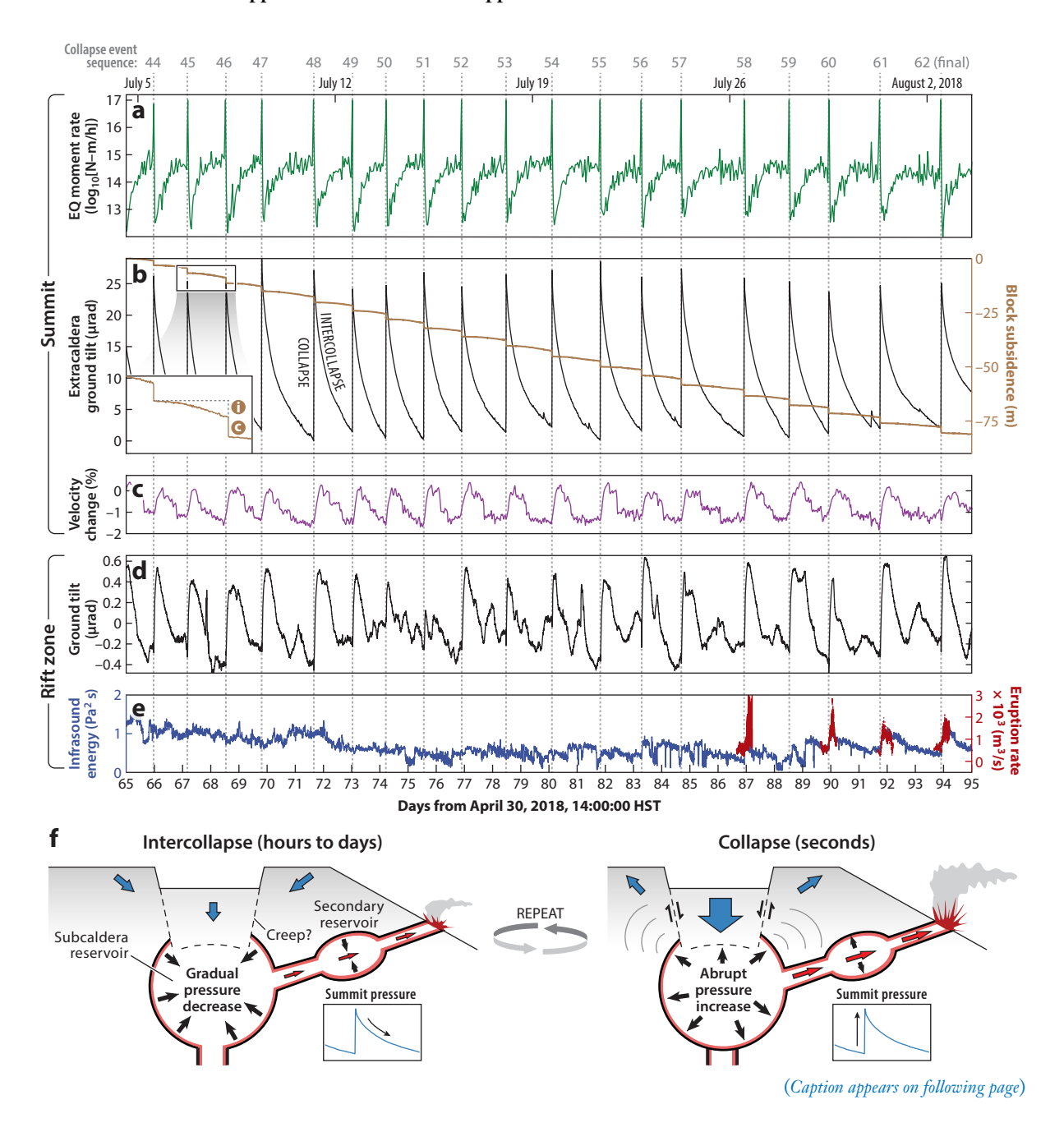
The surface morphology of the caldera evolved greatly throughout the eruption, and changes in geophysical signals were observed—notably around events 19–20 and 55 (Tepp et al. 2020, Anderson & Johanson 2022), likely related to changes in fault geometry—but the basic geophysical character of the collapses remained similar. Their highly repetitive nature indicates a stable (recoverable) process (Neal et al. 2019, Tepp et al. 2020, Anderson & Johanson 2022, Thelen et al. 2022) and was utilized for timing field visits during the eruption. The largest fault block (~1.5 km²) became fully mobile around day 55 after an arcuate fault propagated through the eastern portion of the 1500 CE caldera floor (**Figure 1c**), and subsequently the surface area of collapse grew only modestly, implying that ring faults were well developed during this time.

The caldera's volume grew at a long-term average of 12-13 million m³/day throughout much of Stage 3, reaching a final volume of ~ 825 million m³ (Neal et al. 2019) (**Figure 8**)—smaller than most estimates of erupted volume. Nearly 2,000 M3+ VT earthquakes were cataloged

Volcano-tectonic (VT) earthquake: earthquake caused by brittle rock failure



beneath the summit, along with tens of thousands of smaller events, mostly at <2.5 km depth in a complex distribution of clusters that align closely with the eastern peripheral surface fault but do not clearly outline a complete ring fault structure (Shelly & Thelen 2019, Hotovec-Ellis et al. 2022) (**Figure 10**). Additional information on caldera collapse observations and interpretations is presented in **Supplemental Text Section 4**, and a table of collapse events is presented in **Supplemental Table 1** and **Supplemental Data Set 1**.



1.16 Anderson et al.



Figure 9 (Figure appears on preceding page)

ARjats.cls

One month of caldera collapse cycles recorded at the summit (a-c) and rift (d,e) with conceptual model (f). (a) Hourly seismic moment release rate from the USGS Hawaiian Volcano Observatory catalog (Hotovec-Ellis et al. 2022). Gray numbers show the collapse event sequence. (b) Highpass-filtered caldera-radial ground tilt at station SDH located outside of the caldera and vertical displacement of a GNSS station (CALS) located on a caldera block. Declining intercollapse deformation rates at most tilt and GNSS stations outside of the caldera are well fit with an exponential function with 0.5-d decay time (Anderson & Johanson 2022). The inset shows intercollapse (i) and co-collapse (c) subsidence at CALS more clearly. (c) Relative seismic velocity change at the summit (Hotovec-Ellis et al. 2022). (d) Highpass-filtered northward ground tilt at a station (JKA) located in the LERZ ~30 km from the summit. (e) Median-filtered infrasound energy at the near-vent FIS8 array (Lyons et al. 2021) and bulk eruption rate (Patrick et al. 2019c). Surges are more evident near the end of the eruption but also appeared in June. (f) Simple conceptual model of Stage 3 collapse (ring faults were less complete during Stage 2, and the reservoir vented to the atmosphere). Panels b and f adapted from Anderson & Johanson (2022) (US Geological Survey; public domain). Monitoring station locations are shown in Figure 1. Abbreviations: GNSS, Global Navigation Satellite System; LERZ, lower East Rift Zone.

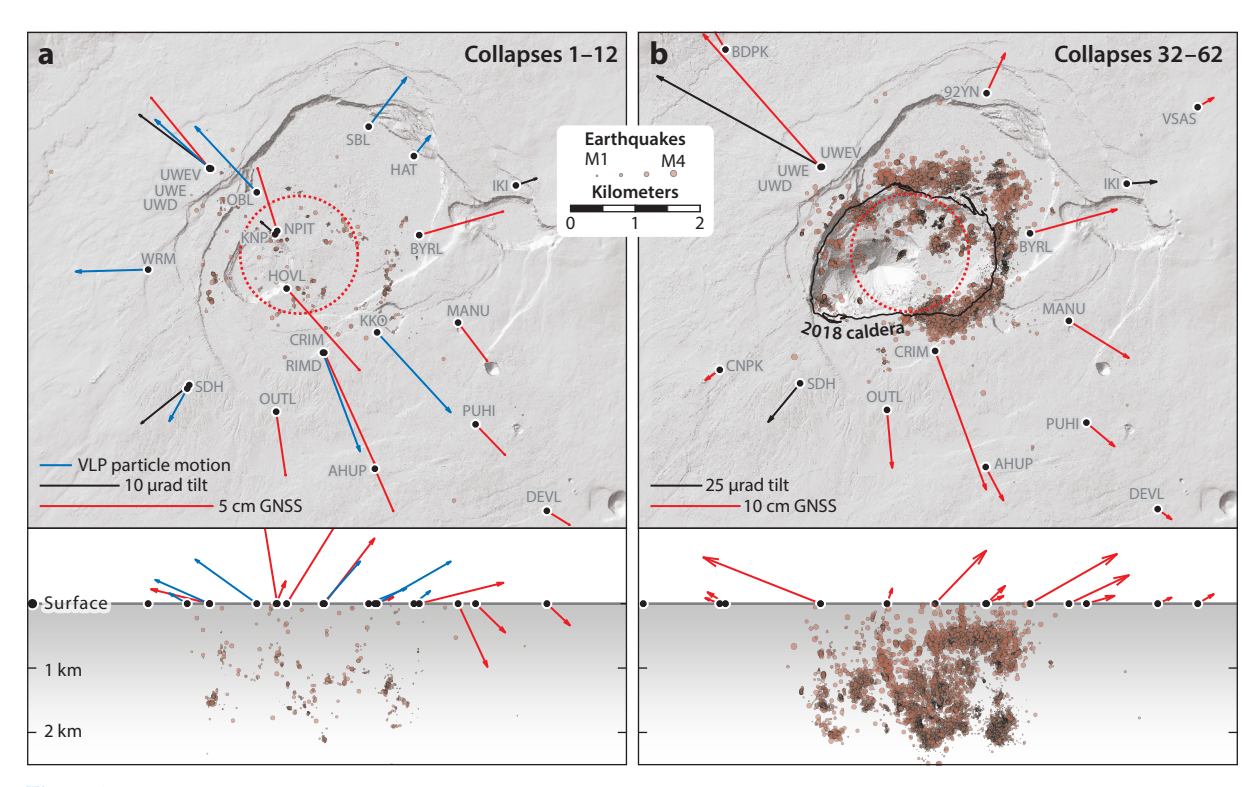


Figure 10

Geophysical data for (a) the first 12 and (b) the last 31 collapses. Vectors show stacked (averaged) co-collapse GNSS displacements, ground tilt (excluding station SMC), and VLP seismic particle motions (Lai et al. 2021, Anderson & Johanson 2022). Three- and four-letter codes (e.g., UWEV) indicate monitoring station names (see Figure 1); only stations located away from collapsing caldera blocks are shown. Near-field seismometers clipped during the latter collapses and are not shown. Dots show relocated earthquakes between collapses from Shelly & Thelen (2019). Almost all summit seismicity was located within the 1500 CE caldera. Background digital elevation models show pre-collapse topography (panel a, 2009) and post-collapse topography (panel b, 2018). Red circles show approximate Halema'uma'u reservoir geometry inferred by Anderson et al. (2019). Cross sections show earthquakes collapsed onto an east-west plane with depth relative to ~1,100 m asl, and east-versus-vertical GNSS displacements and VLP motions (some vectors truncated). Supplemental Movies show animations. Abbreviations: GNSS, Global Navigation Satellite System; VLP, very long period.

To first order, observations are consistent with a simple conceptual model first proposed for historical basaltic collapses and further developed for Kīlauea (e.g., Simkin & Howard 1970, Kumagai et al. 2001). Magma outflow to the ERZ gradually depressurized the subcaldera magma reservoir (HCR), reducing support for roof rock. The rock eventually failed along ring faults (blind faults during Stage 2 and throughgoing during Stage 3), permitting a piston-like mass (or masses) to abruptly subside downward, pressurizing the magma, and stabilizing the roof block. Over the subsequent hours to days, magma outflow gradually reduced reservoir pressure and eventually the roof rock failed again, beginning a new cycle. This conceptual model was used to inform hazards assessments during the eruption (Neal & Anderson 2020), but few models existed at the time to quantitatively relate collapse processes with observations.

Observations from 2018 now yield an opportunity to quantitatively investigate the mechanism, geometry, and physical properties of the collapse and subcaldera reservoir. Point-source moment tensor inversions of co-collapse VLP seismic data are consistent with pressure increase in a shallow source together with slip along steeply dipping faults (Lai et al. 2021, Soubestre et al. 2021). Physics-based models—which better capture collapse processes—indicate that a combination of slip on ring faults, ramp-like reservoir pressurization, and momentum changes of the roof block and reservoir magma can explain most features of co-collapse geodetic and seismic observations (Segall et al. 2019, 2020; Wang et al. 2022). Models suggest that Stage 2 and 3 collapses increased reservoir pressure by roughly 0.5 MPa and 2-3 MPa, respectively, but require assumptions about reservoir geometry (Segall et al. 2020, Anderson & Johanson 2022, Wang et al. 2022). These pressure changes may explain the post-collapse ejection of tephra plumes, rift zone surges (Section 3.2.1), upward-and-outward displacement of the ground around the caldera, release of VLP seismic energy, and (together with shaking-induced host rock damage) temporary increases in summit seismic velocities of >1% during the first 4-5 h after collapses (Wu et al. 2020, Hotovec-Ellis et al. 2022). Collapse-induced increases in reservoir pressure did not, however, fully recover loss during the pre-collapse period, implying residual frictional strength on ring faults (Anderson et al. 2019, Anderson & Johanson 2022).

Between episodic collapses, subsidence and contraction of the broader summit region can be attributed chiefly to magma evacuation from the HCR and imply a near-complete reduction of excess eruptive (driving) pressure during each cycle (Anderson & Johanson 2022, Segall et al. 2022). Concurrent creep on ring faults may explain caldera block subsidence and VT seismicity between collapses (Tepp 2021, Wang et al. 2023); models suggest spatially heterogeneous frictional properties and possibly a viscous rock rheology above the reservoir (Wang et al. 2023). In contrast, VT earthquakes located away from ring faults may have been generated by another mechanism, such as shear and closure of cracks related to reservoir depressurization (Shelly & Thelen 2019). The dominance of VT earthquakes in the eastern portion of the caldera may also suggest an asymmetrical process, in which co-collapse slip was concentrated in the northwestern portion of the caldera while ring faults to the southeast slipped both between and during collapses (Shelly & Thelen 2019, Lai et al. 2021); GNSS data, however, place limits on any asymmetry (Wang et al. 2023). Regardless, preexisting structures—including the lava lake vent, hydrothermal features (Soubestre et al. 2021), and older caldera faults—almost certainly played an important role in the evolution of collapse. In some areas, for instance, collapse may have utilized faults formed during the much larger collapse in 1500 CE, whereas fault slip along the eastern sector cut a thick sequence of lava flows filling that older caldera.

Dynamical piston-like collapse models that invoke rate-dependent ring fault friction and pressure-dependent magma outflow can predict cycles of collapses (Roman & Lundgren 2021, Segall & Anderson 2021). These models demonstrate that vent elevation plays a critical role in the onset of caldera collapse and that collapse events sustain large eruptions. The models can also

т т8 Anderson et al.



be used to constrain reservoir volumes (Section 3.1) and frictional properties of the ring faults, with important implications for understanding earthquakes in nonvolcanic settings. However, the role of the SCR in the 2018 collapse process has been debated, and some other kinds of models have utilized dike-like reservoir geometries and argued that collapse-induced volatile resorption was important during Stage 2 (Soubestre et al. 2021).

2.3.3. Tephra explosions. The geologic and historical records at Kīlauea include numerous tephra-forming eruptions (explosions), including lethal events in 1790 and 1924. Their mechanisms have been debated and are probably varied (e.g., Houghton et al. 2011, Orr et al. 2013, Fiske et al. 2019), but a steam-blast interpretation by Stearns (1925) (Supplemental Figure 9) has been widely accepted for explosions that occurred in 1924.

Several mechanisms produced tephra emissions and explosions at Kīlauea's summit in 2018. First, as the lava lake drained, destabilized conduit walls collapsed onto its surface, producing small explosions and juvenile-rich tephra—similar to many events over the preceding decade (Carey et al. 2012, Orr et al. 2013). The largest, on May 9 (day 9), ejected ~230 m³ of material, consisting of about 5% wallrock clasts and 95% pumice lapilli, bombs, and glassy ash. Tephra was also produced by weak background venting, punctuated by periods of more vigorous activity likely triggered in part by rockfalls into the collapsing conduit, that continued into early June after the demise of the lava lake.

Of more concern in 2018 was the possibility that phreatic or phreatomagmatic explosions could occur as summit magma drained toward the elevation of the water table, allowing groundwater to penetrate cooling conduit walls (Neal & Anderson 2020), as Stearns (1925) had suggested for 1924. [Indeed, the nearby presence of groundwater was later confirmed by the formation of a water lake in the post-2018 caldera (Section 2.4).] Beginning shortly after the lava lake disappeared, a series of explosions ejected ballistic wallrock blocks several tens of centimeters across (Supplemental Figure 10) and sent ash plumes as high as 8 km above the vent (Figure 6a). These explosions were the largest at the volcano since 1924, and ash fell at least 50 km downwind. Isopachs of the cumulative 2018 tephra deposit indicate a total volume of at least 4.2×10^5 m³ (a tiny fraction of the erupted lava volume), with predominant dispersal by trade winds toward the southwest, thinning from 5 cm proximally to <2 mm at 6 km from the vent (S. Isgett, unpublished map).

In one of the most surprising outcomes of the 2018 eruption, however, it was recognized that observations did not support a mechanism for these events involving external water (steam) (Neal & Anderson 2020). First, tephra plumes appeared visually at the caldera floor \sim 20–30 s after the start of each early-stage collapse event (Crozier et al. 2018). Second, post-lava-lake ash consisted overwhelmingly of wallrock material, with fresh glassy components sparse or, more generally, absent. Although some deposits locally contain accretionary lapilli and vesicles, they are inconsistently distributed crosswind and downwind and likely record rainfall contemporaneous with ashfall. Finally, SO₂ emission rates during this period were generally similar to pre-2018 values, except for a fortuitous measurement following a collapse event on May 23 that was two to three times higher (Kern et al. 2020) (Figure 6)—inconsistent with scrubbing of SO₂ by groundwater or steam.

These explosions are now thought to be closely related to failure of the shallow magma system. As caldera collapse events abruptly increased magma system pressure, previously exsolved gases were forced upward through the rubble-filled conduit, filtering out juvenile material and entraining fragmented wallrock (Neal et al. 2019, Shelly & Thelen 2019, Kern et al. 2020) (Figure 11). Plume simulations driven by collapse-induced reservoir pressurization can reproduce observed heights and ascent times, and indicate that plumes were buoyancy dominated and strongly affected by wind (Crozier et al. 2018). These results are consistent with calculations that groundwater

Historical record:

written accounts of volcanic activity at Kīlauea begin with the visit of Ellis in 1823, but Hawaiian oral traditions metaphorically describe hundreds of years of activity



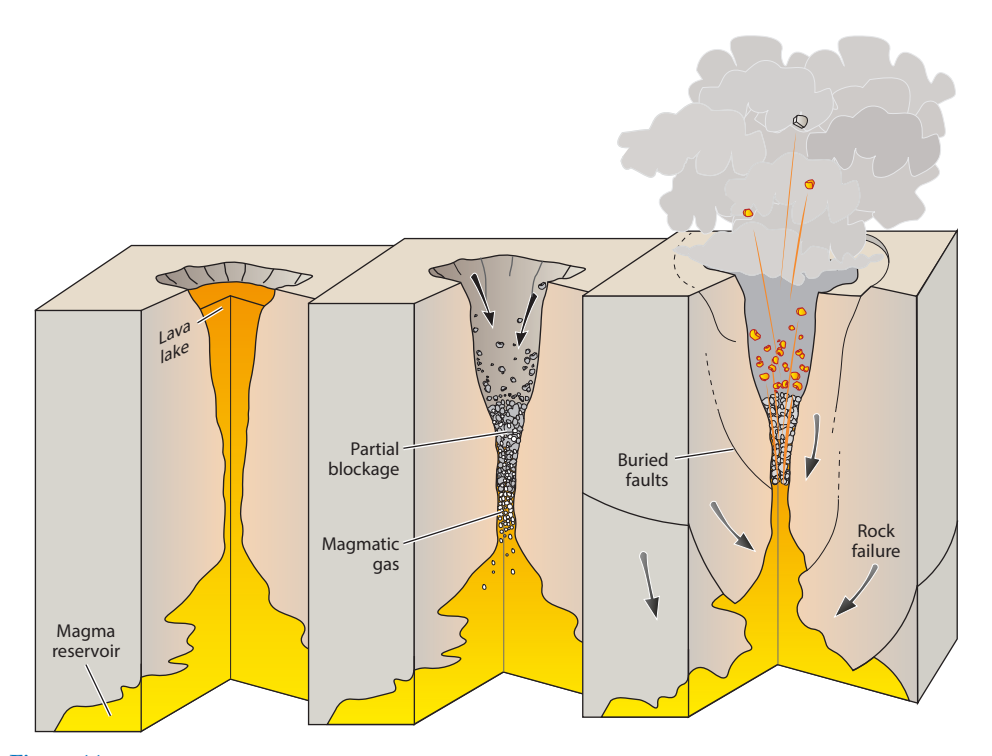


Figure 11

Proposed conceptual model for collapse-induced explosions [sometimes called collapse/explosions (Neal et al. 2019, Neal & Anderson 2020)] at Kīlauea in 2018. Removal of magma from the reservoir caused the lava lake to subside and the conduit to partially collapse. Reduction in magma pressure eventually caused host rock failure, which abruptly intruded into the reservoir, increasing its pressure and forcing exsolved volatiles upward through the rubbly conduit, entraining tephra. Figure adapted from an illustration of the Stearns (1925) conceptual model in Mastin et al. (1999) (US Geological Survey; public domain).

would have been prevented from directly interacting with magma by the preheated rock around the conduit (Hsieh & Ingebritsen 2019). More complete collapse of the vent, as well as a receding magma surface, reduced and ultimately blocked tephra and gas emissions around the Stage 2–3 transition (Neal & Anderson 2020).

2.4. End of the Eruption and the Post-2018 Period

By July 2018, despite some gradual, long-term reductions in deformation rates, SO₂ emission rates, and lava eruption rates (Kern et al. 2020, Dietterich et al. 2021, Anderson & Johanson 2022), the eruption appeared to have entered a stable regime and there were no indications at the time that it was nearing its end (Neal & Anderson 2020, Tepp et al. 2020). Yet, the summit collapse on August 2 (day 94) would prove to be the last. Within days, earthquake rates had dropped by two orders of magnitude (Wei et al. 2022), eruption rates had dwindled to near zero, and the eruption was effectively over. Understanding these processes is of obvious importance for better characterizing hazards during future eruptions.

One obvious possibility—that the summit ran out of eruptible magma—appears to be ruled out by a caldera volume that was smaller than the inferred HCR (Anderson et al. 2019) and by post-2018 observations indicating remnant magma in that reservoir (**Supplemental Text Section 6**). The relative stability of the collapse cycles also suggests that the system could have supported more

1.20 Anderson et al.



collapses (e.g., Roman & Lundgren 2021). Low eruptive driving pressure inferred in some studies (Anderson & Johanson 2022, Segall et al. 2022) implies that the eruption was sustained (perhaps tenuously) by summit collapses; if correct, any interruption to the summit collapse process (e.g., a stuck piston) could have terminated the eruption—an event that would have been difficult or impossible to forecast. Pressure in the SCR had also gradually declined for weeks, and although its role in driving the eruption remains debated, Roman & Lundgren (2021) suggested that pressure eventually became too low to keep its connection with the HCR open. Magma connections may also have been severed by the summit collapses themselves, or by a structural failure along the magma flow path.

The long-term response (recovery) of the volcanic system will further elucidate changes wrought by the 2018 eruption. Through the time of writing, the post-2018 period has included the formation of Kīlauea's first summit water lake in written history, reinflation of the summit and ERZ storage systems, high rates of south flank motion, months-long dominantly effusive summit eruptions (**Supplemental Figure 11**), a dramatic increase in the rate of deep Pāhala earthquakes [beginning about a year after the eruption (Wilding et al. 2023)], and the first eruption at neighboring Mauna Loa in 38 years. Kīlauea's post-2018 eruptions appear to be fed from the shallow HCR and may suggest refill with similar but slightly more mafic (primitive) magma, supporting the notion that the 2018 collapse significantly disrupted magma pathways but did not fundamentally alter the basic structure of the reservoir (Lynn & Swanson 2022). The post-eruptive period is discussed more fully in **Supplemental Text Section 6**.

3. SYNTHESIS AND INFERENCES

3.1. Magma Storage

The volumes and locations of stored magma govern eruptive activity and hazard, but they are poorly known at most of Earth's volcanoes. The diversity of observations captured during and following the large-scale, rapid draining of Kīlauea's summit-rift magma system provides one of the best opportunities for resolving magma storage beneath any volcano.

At the summit, geodetic data indicate that magma was withdrawn chiefly from the HCR and the SCR (Anderson et al. 2019, Roman & Lundgren 2021, Anderson & Johanson 2022), and petrologic data (Section 3.2.2) are consistent with these ideas. However, despite decades of study, the SCR has remained very poorly understood, while the HCR has been interpreted variously as a roughly equant body or a set of intersecting dike- and/or sill-like magma bodies, and estimates of its volume have varied over two orders of magnitude (e.g., Baker & Amelung 2012, Dawson & Chouet 2014, Poland et al. 2014, Anderson et al. 2015, Pietruszka et al. 2015).

Joint inversion of lava lake elevation and geodetic data can be used to resolve the geometry of the subcaldera reservoir (HCR). Inversions during the pre-collapse period (Stage 1) are consistent with steady depressurization of magma in a spheroidal, slightly prolate, vertical reservoir located just east of the former Halema'uma'u crater, centered at a depth of ~2 km (Anderson et al. 2019). Globally, magma reservoir volumes are challenging to estimate, but 2018 data yield a pre-collapse volume of 2.5–7.2 km³ (at 68% confidence) (Anderson et al. 2019), consistent with estimates from physics-based caldera collapse models [roughly 1–10 km³ (Roman & Lundgren 2021, Segall & Anderson 2021, Wang et al. 2022)]. The geophysically inferred reservoir geometry agrees closely with the surface expression of the 2018 collapse and implies that the caldera roof block was relatively thin and wide, affecting both the onset and style of collapse (Anderson et al. 2019). These results are inconsistent with very small reservoir volumes suggested by some previous geochemical studies [<0.2 km³ (Pietruszka et al. 2015)] unless the melt-dominated, circulating core of the reservoir is much smaller than the overall volume (Pietruszka et al. 2015, Garcia et al. 2021)—an

idea that would also need to be reconciled with the much larger caldera volume. Models suggest HCR magma compressibilities of roughly 2×10^{10} to 20×10^{10} Pa⁻¹, consistent with the presence of an exsolved bubble phase (Segall et al. 2020, Anderson & Johanson 2022).

Other data sets suggest additional geometrical complexity. VT earthquakes lie mostly but not entirely outside the inferred pre-collapse reservoir and do not clearly delineate a spheroidal aseismic zone (Shelly & Thelen 2019). VLP seismic data recorded in 2018 have been interpreted in the context of both spheroidal and dike-like reservoir models, and also tend to favor modestly shallower sources (Crozier et al. 2018, Liang & Dunham 2020, Crozier & Karlstrom 2021, Lai et al. 2021, Soubestre et al. 2021). Generally, geodetic data and caldera geometry probably cannot rule out storage in a network of tabular bodies rather than a more contiguous spheroidal geometry. However, the stability of summit lava bulk MgO content (7-7.5 wt%) and eruption temperatures over most of the 2008-2018 lava lake's life (Thornber et al. 2015, Lynn 2022) (Figure 3; Supplemental Figure 12) indicate that the HCR must be thermally insulating, spatially continuous, and large enough to allow compositional buffering as the summit reservoirs were continuously tapped by the ERZ (Pu'u'ō'ō) transport system. The regularity of the collapse sequence might also be difficult to explain with a highly irregular subcaldera reservoir.

Relatively little work has yet been done using 2018 data to resolve the SCR. Co- and posteruptive geodetic data have been modeled using both spherical and sill-like reservoir geometries, respectively, at ~3–4 km depth (Roman & Lundgren 2021, Wang et al. 2021), resulting in a poorly resolved volume of perhaps tens of km³ (Roman & Lundgren 2021).

In the ERZ, stored magma can serve as the source for subsequent intrusions and can affect eruption dynamics, but the geometries, compositions, and longevity of such bodies have previously been poorly known. The 2018 eruption revealed a large, rift-aligned storage zone extending kilometers along the MERZ. Co- and post-eruptive surface deformation can be explained by contraction and expansion, respectively, of tabular (dike-like) or other rift-parallel bodies extending both uprift and downrift from Pu'u'ō'ō at shallow depths (mostly <3 km) (Chen et al. 2019, Neal et al. 2019, Kundu et al. 2020, Wang et al. 2021) (Figure 5d). The spatial scale and magnitude of deformation observed during the first 2-3 days of the eruption require a relatively large quantity of highly mobile magma and imply that a barrier to downrift flow existed near Pu'u'ō'ō in the years before 2018 (Patrick et al. 2020). The presence of magma storage in the MERZ is also suggested by the delay between the onset of downrift magma propagation and summit subsidence (Townsend & Huang 2022) and observations of collapse-induced pressure surges in the rift (next section).

In the LERZ, the compositions of Stage 1 and 2 lava (Figure 7a) can be explained by the presence of a complex, variably fractionated magma body or bodies ~2 km beneath the vents, likely remaining from the 1955/1960 intrusions. This melt was tapped, remobilized, and gradually mixed with and brought to the surface by magma from the 2018 intrusion (Gansecki et al. 2019, Wieser et al. 2022). As activity focused at fissure 8, most LERZ-stored magmas had already been flushed out by newly arrived magma from uprift (Gansecki et al. 2019, Wieser et al. 2022) (Section 3.2.2).

The question of magma storage in the deep rift zone has not yet been addressed in detail using 2018 data, although melt inclusion barometry indicates that erupted lavas were generally sourced from <5 km depth (in contrast to eruptions in 1959 and 1960, for instance) (Lerner et al. 2021, Wieser et al. 2021).

3.2. The Coupled Summit-Rift Magma Transport System

Volcano and eruption dynamics are governed in large part by the transmission of pressure changes that drive the flow of magma. Geophysical, field, gas emissions, and petrological/geochemical observations over previous decades at Kīlauea revealed that pressure changes propagated rapidly between the HCR and MERZ, and that the HCR and lava lake were continuously tapped by the

Anderson et al. I.22



transport system to Pu'u'ō'ō (either directly or via the SCR) (e.g., Thornber et al. 2015, Patrick et al. 2019a). Yet, the geometry of this connection—and particularly the role of the SCR—has remained enigmatic, impairing efforts to interpret data and assess changing hazards at the volcano.

3.2.1. Driving pressure, caldera collapse, and the Halema'uma'u-East Rift Zone connection. Abundant evidence from 2018 relates pressure in the HCR with pressure at the LERZ eruptive vents, further elucidating a tightly coupled system.

Post-collapse pressure surges along the length of the ERZ, analogous to water hammers in pipes, were a key discovery (Patrick et al. 2019c, Sigmundsson 2019) (Section 2.2.2; Figure 9). Collapses served as impulsive perturbations of the entire shallow magma system, with variations in eruption rate and ground deformation as observed outputs. Following ideas developed during the Pu'u'ō'ō eruption (Montagna & Gonnermann 2013, Haney et al. 2016), the delay between collapses and peak eruption rates (~2-4 h) appears to reflect a time-dependent balancing of pressure along the magma path between the HCR and the vent, in which magma flowed through an intermediary storage zone in the ERZ (or possibly the SCR) and/or an elastic-walled dike (Patrick et al. 2019c, Segall et al. 2022). A tripling of eruption rate during surges in 2018 implies that excess magma pressure (to which eruption rate was proportional) driving the eruption was low: likely <1-2 MPa at the end of each collapse cycle (Anderson & Johanson 2022, Segall et al. 2022).

Changes in lava lake surface elevation further support the notion of a low eruptive driving pressure and a tightly coupled summit rift system. In the days before the eruption began, the surface of Kīlauea's lava lake was 800 m above the elevation of the eventual LERZ vent, implying ~20 MPa of potential excess pressure to drive an eruption 40 km distant. Magma pressure at that time was efficiently propagated through the well-established MERZ conduit as far as Pu'u'ō'ō (20 km), evidenced by a small lava pond only ~170 m lower than the summit lava lake (Patrick et al. 2019a, 2020). After the 2018 eruption began, pressure in the HCR fell by \sim 17 MPa during Stage 1 (Section 2.3.1), leaving just ~3 MPa of excess pressure at the onset of caldera collapse (Anderson et al. 2019, Segall et al. 2022). Thus, excess driving pressure at the summit must have been low throughout the eruption and caldera collapse must have served to maintain this pressure. The role of the SCR in driving the eruption, however, remains unclear (Section 3.2.3).

Magma flow rates indicate an increasingly tight HCR-vent connection as the eruption progressed. During Stage 1, geophysically estimated magma evacuation rates from the HCR were much higher than eruption rates $[\sim 35-70 \text{ m}^3/\text{s} \text{ versus} \sim 7 \text{ m}^3/\text{s} \text{ (Anderson et al. 2019, Dietterich$ et al. 2021)] as magma pathways evolved and the LERZ intrusion grew. These rates increased and became more similar as the eruption progressed, and both decreased dramatically after the last collapse event. The onset of caldera collapse (Stage 2) was also nearly coincident with the cessation of the LERZ dike opening and the eruption of more primitive lava at high rates from LERZ fissures (**Figure 6c**), hinting at a close physical relation between summit and rift.

Caldera collapse increased reservoir pressure through release of the gravitational potential energy of the roof block, which drove large volumes of magma out of the summit (e.g., Druitt & Sparks 1984, Gudmundsson 2015, Roman & Lundgren 2021, Segall & Anderson 2021). The onset of caldera collapse thus represents a critical turning point in an eruption, theoretically allowing mobilization of nearly all eruptible subcaldera magma (for a given vent height) (Anderson et al. 2019, Roman & Lundgren 2021, Segall & Anderson 2021). In this way, Kīlauea's 2018 eruption continued for months in what may have been a delicate balance between withdrawal-induced reservoir depressurization and collapse-induced repressurization. This process resulted in erupted volumes an order of magnitude larger than those observed historically from vents at comparable elevations that did not trigger summit collapse (Epp et al. 1983) (Figure 12).

Excess driving pressure: magma pressure in excess of magmastatic, which drives flow



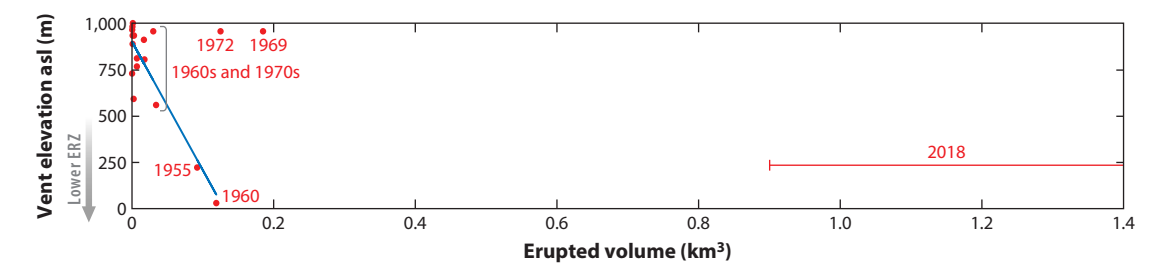


Figure 12

Mean vent elevation versus erupted volume for Kīlauea eruptions from 1955 to 2018 (excluding the 35-year-long Puʻuʻōʻō eruption) with linear fit (*blue line*; excluding 1969, 1972, and 2018). Outliers in 1969 and 1972 were related to the long-lived Maunaulu eruption, which was more strongly influenced by magma resupply. Data from Epp et al. (1983) and Dietterich et al. (2021). Abbreviation: ERZ, East Rift Zone.

3.2.2. Origin of the 2018 lavas. The close pressure coupling described above does not necessarily require physical advection of magma all the way from summit to vent. Early 2018 lavas were likely sourced from remobilized ERZ magma, but the source of the more voluminous Stage 3 lava has been debated.

Several lines of evidence suggest that Stage 3 lavas were sourced from primitive magmas that passed through the summit reservoir system not long before the eruption. First, Stage 3 lavas exhibit broad geochemical similarities with pre-2018 summit lavas (Gansecki et al. 2019). Second, Stage 3 lavas contain high-Fo (>Fo₈₇) olivine (Gansecki et al. 2019, Lerner et al. 2021, Wieser et al. 2021, Mourey et al. 2022), which formed in primitive melts (MgO > 12 wt%, T > 1,300°C) (Figure 7) and had not been seen in high abundance at Kīlauea since 1974 (Vinet & Higgins 2010, Lynn et al. 2017, Lynn & Swanson 2022). Wieser et al. (2019) proposed that high-Fo olivine was stored in a crystal mush below the summit over decadal timescales prior to remobilization in 2018. However, Mourey et al. (2023b) argued that element diffusion during high temperature storage for more than a few years would likely have erased the high-Fo signal and imparted deformation structures to the olivine that were not observed (Gansecki et al. 2019)—indicating rather that the olivine entered the summit or ERZ in primitive melts a few months to years before eruption, consistent with diffusion chronometry timescales (Mourey et al. 2022). Finally, trapping depths estimated from erupted melt inclusions are consistent with crystallization in storage reservoirs at the summit (low-Fo olivine at \sim 1–3 km in the HCR and high-Fo olivine at 3–5 km in the SCR) (Lerner et al. 2021, Wieser et al. 2021) (Supplemental Figure 13). Although 1-5 km depths are also consistent with storage in the rift zone, low sulfur concentrations and isotopically light δ^{34} S signatures found in melt inclusions indicate degassing and recycling during convection and drainback in the 2008–2018 summit lava lake (Lerner et al. 2021). Trapping depths can also be reconciled with deep-derived primitive melt if crystallization of high-Fo olivine occurred while the melts circulated in the SCR.

Alternatively, Pietruszka et al. (2021) proposed that Stage 3 lavas were sourced not from the summit but from magma stored in the ERZ downrift of Puʻuʻōʻō that mixed with summit-derived magma over the decade preceding the 2018 eruption. These ideas are based on observations that Stage 3 basalts have relatively high K₂O and TiO₂ at a given MgO value, high Nb/Y ratios, and low CaO/TiO₂ and Sr/Zr ratios compared to pre-2018 Puʻuʻōʻō and summit lava lake lavas. An ERZ source for the Stage 3 lavas requires the accumulation of large quantities of magma in the rift zone and implies that summit magma replaced rift-stored magma rather than erupting in 2018. However, distinguishing parent magmas based on subtle geochemical differences is challenging,

K₂O and TiO₂:

minor-element
contents that can be
measured rapidly and
used to track changes
in parental magma
composition and
characterize magma
evolution due to
fractional
crystallization of
olivine ±
clinopyroxene ±
plagioclase

Nb/Y: a ratio of niobium, a highly incompatible element, over yttrium, a moderately incompatible element that is insensitive to fractional crystallization of olivine and thus better reflects changes in parental magma composition (e.g., mantle source composition)

1.24 Anderson et al.



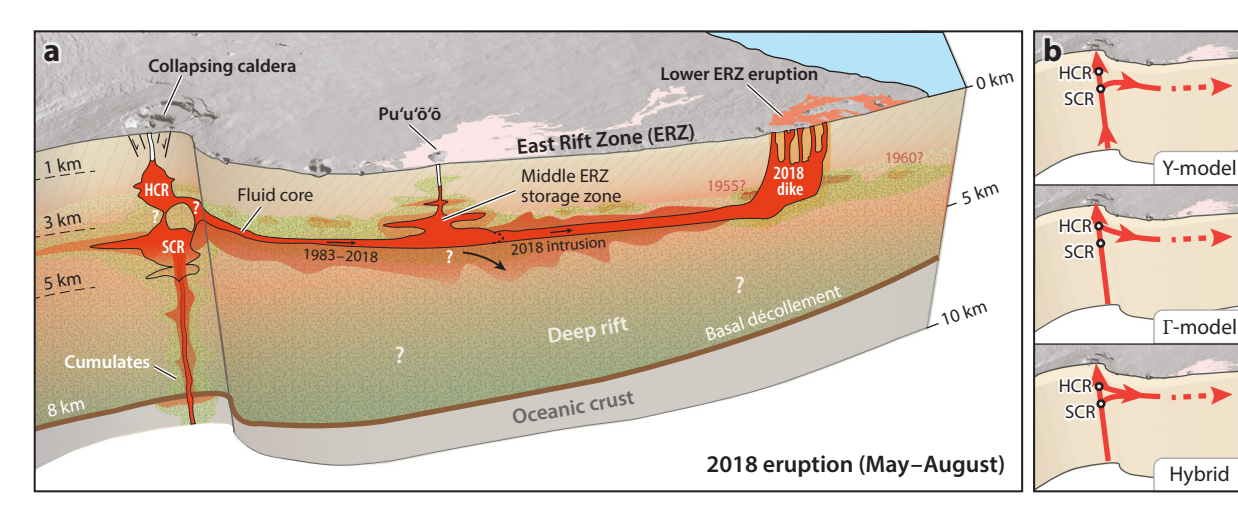


Figure 13

Conceptual model of Kīlauea's summit and ERZ. The figure is vertically exaggerated. (a) Cross section showing magma migration during the 2018 eruption. Panel a adapted from Poland et al. (2014) and Gansecki et al. (2019); reprinted with permission from AAAS. (b) Several proposed connection geometries between the summit reservoirs and the ERZ. Abbreviations: ERZ, East Rift Zone; HCR, Halema'uma'u crater reservoir; SCR, south caldera reservoir.

and it is not clear how this model can explain the presence of high-Fo olivine in Stage 3 lavas (Mourey et al. 2022).

3.2.3. The enigmatic summit-rift magma transport pathway and role of the south caldera reservoir. Before 2018, two general models for the summit-rift magma system had emerged: the Γ-model (gamma), in which the ERZ is connected to the summit storage system through the HCR, and the Y-model, in which it is connected through the SCR (Cervelli & Miklius 2003; Poland et al. 2014, 2021b) (Figure 13). The 2018 eruption raised new questions and provided numerous, sometimes apparently contradictory, clues.

As described in Section 3.2.1, pressure changes in the HCR were closely related to changes in the rift zone. Indeed, models of geodetic and seismic data during the first days of magma intrusion into the LERZ (Townsend & Huang 2022) and geodetic data during the post-eruptive period (Wang et al. 2021) both suggest that the HCR was directly and efficiently coupled with the rift zone (probably via an ERZ reservoir), whereas the SCR-rift connection was weak or possibly nonexistent. Some caldera collapse models are also consistent with a direct HCR-vent connection (Segall & Anderson 2021, Anderson & Johanson 2022).

In contrast, Roman & Lundgren (2021) argued that the HCR was connected to the rift zone through the SCR (Y-model), although based on part on a geodetic station (UWD) that may not have been representative of pressure in the magma system (Anderson & Johanson 2022). Wieser et al. (2021) also proposed that low-Fo olivine HCR magma may have drained into the SCR and mixed with its high-Fo cargo before continuing into the ERZ. However, entrapment depths are broadly consistent with both the reservoirs (Lerner et al. 2021, Wieser et al. 2021), making this distinction difficult.

Post-eruptive geodetic data have been interpreted in the context of a relatively strong connection between the two reservoirs, but gradually decaying rates of ground subsidence related to the SCR were not evidently affected by the summit collapse and continued for at least 300 days after the end of the eruption, whereas magma began accumulating in the HCR region beginning ~100 days after the end of collapse (Poland et al. 2019, Wang et al. 2021, Anderson & Johanson

CaO/TiO2 and **Sr/Zr:** geochemical ratios that are sensitive to the fractionation of plagioclase and can help discriminate less evolved summit magmas from more evolved rift-stored magmas at Kīlauea



2022). Qualitatively, these observations may suggest rather that reservoirs were only poorly coupled with one another, and possibly that the SCR was a passive participant in 2018, with its magma perhaps entering the deep rift zone but not erupting.

Most likely, simple existing models do not adequately account for the complexity of the summit magma system nor magma transport through a heterogeneous rift zone containing strong spatial variations in melt fraction. However, Denlinger (2019) showed that a three-dimensional multiphase porous flow model can predict evolving co- and post-eruptive deformations, and implies an ophiolite-like rift zone structure with pressure changes occurring at >2 km depth. Studies of this kind represent an important step beyond the simple models typically used to interpret geodetic data and a physically consistent way to couple evolving summit and rift pressures and flow rates.

3.3. Placing 2018 in the Broader Context of Kīlauea's Past

In a conceptual model for the long-term growth of Kīlauea, gradual accumulation of magma pressure, coupled with gravitational stress and rift zone intrusions, drives slow seaward flank motion away from Kīlauea's buttressed north flank, stressing the décollement. Large flank displacements release this stress, open the rift zone(s), and depressurize the magma system, which may result in large-scale summit collapse and/or explosions. Eruptions may become smaller and less frequent in subsequent years, but magma pressure gradually recovers and gravitational stress accumulates, eventually resulting in another slip event. In this way, the volcano grows through coupled, possibly periodic, cyclical magmatic-tectonic processes, and slip on the basal décollement accommodates the volcano's growth (Dieterich 1988, Denlinger & Morgan 2014, Montgomery-Brown & Miklius 2020).

In broad strokes, events of 2018 appear consistent with this general model. Yet, while previous summit lowerings at Kīlauea (a nongenetic term for significant subsidence or collapse events) are believed to have been triggered by magma withdrawal from summit reservoirs to feed rift zone intrusions and/or eruptions (Supplemental Text Section 2)—and are thus controlled in part by rift zone tectonics—they have also occurred in the absence of known large flank earthquakes [e.g., 1840 (Wright & Klein 2014)] and may be controlled in part by reductions in magma supply rate (Swanson et al. 2014). Thus, the relation between summit lowering events, rift zone tectonics, and magma supply is likely complex.

An important question is to what extent lowerings affect the connectivity and stability of Kīlauea's magma storage and supply system. Geochemical variations in tephras and lavas erupted over the last 500+ years indicate that these impacts can be significant (Lynn & Swanson 2022). Low-Fo olivine (e.g., <Fo₈₂) and low-MgO glasses (e.g., <7.0 wt%) that preceded significant lowering events (e.g., 1500, possibly 1790, and 1924) reflect a system in which incoming mafic melts are buffered in a relatively large, mature, and stable reservoir. After lowering events, high-Fo olivine (e.g., >Fo₈₇) and high-MgO glasses (e.g., >9.0 wt%) reflect either a disrupted reservoir system in which incoming primitive mantle melts do not undergo significant evolution prior to eruption or a period of low magma supply in which large reservoirs are slow to recover.

This pattern was repeated in the years prior to and after the 2018 eruption. Between 2008 and 2018, summit lavas were dominated by low-Fo olivine (e.g., Thornber et al. 2015, Lynn 2022), while lava erupted from the LERZ in 2018 and the summit in 2020 and 2021 contained a significant proportion of high-Fo olivine (e.g., Lerner et al. 2021, Wieser et al. 2021, Lynn 2022, Mourey et al. 2022) (Supplemental Text Section 6). These relatively abrupt changes in olivine major element chemistry indicate that the summit collapse perturbed the reservoir system—perhaps through advective stirring—and enabled the high-Fo olivine to escape the reservoir. However, the overall compositions of post-2018 lavas was similar to that of pre-2018 lavas (Lynn 2022), suggesting that magma storage and transport pathways were disrupted but not fundamentally changed.

1.26 Anderson et al.



Major summit collapses in ca. 200 BCE and ca. 1500 CE were closely related to transitions from dominantly effusive to explosive eruption styles that lasted for centuries (Swanson et al. 2014). The 2018 collapse was much smaller than these events, and was probably more similar to (although larger than) the summit lowerings common in the nineteenth century, which did not result in fundamental changes in Kīlauea's eruption style (Wright & Klein 2014). To date, there is also no evidence of a general transition from effusive to intrusive behavior as occurred following the 1975 south flank earthquake (Cayol et al. 2000).

4. SUMMARY, OPEN QUESTIONS, AND OUTLOOK

In this section we summarize findings, highlighting points of particular interest and outstanding questions. We also suggest some possible avenues of future research.

4.1. Summary of Key Findings

Major volcanic eruptions are often preceded by significant unrest and a rapid buildup to failure, typically driven by magma system pressurization or the migration of magma to shallow depths. In contrast, unrest in the months preceding the 2018 eruption was minor compared with the scale of the eruption, and pressure in the subcaldera magma reservoir (HCR) was not much higher than lithostatic (dike propagation may occur at lower pressures), with the caveat that pressure in the SCR is largely unknown. Rather, the stage was set for Kīlauea's 2018 eruption by the accumulation of decades of gravity-induced opening stress on the rift zone as well as gradual magma pressurization due to the accumulation of stored magma. The system was then brought more rapidly to failure by only a modest backup in the shallow ERZ magma system and, possibly, an increase in magma supply to the volcano.

Intrusion of magma into Kīlauea's LERZ triggered a large (~Mw7) décollement earthquake, which released stress accumulated in the offshore portion of the décollement by gravitational creep and previous intrusions into the ERZ. The earthquake in turn appears to have promoted magma flow and further opening of the intrusion. Downrift flow drained magma first from the MERZ and shortly thereafter the summit. The low elevation of the eruptive vents—and possibly rift opening due to the décollement earthquake—permitted more complete draining of the summit system, leading to the onset of caldera collapse as roof rock began to subside into the HCR. The eruption demonstrated that caldera collapses at basaltic shield volcanoes may begin after withdrawal of only a few percent of stored magma.

Detailed observations of caldera collapse at Kīlauea are globally unique and have enabled a leap forward in understanding. During collapse, reservoir roof rock subsided episodically into the subcaldera reservoir (HCR) under the force of gravity, pressurizing it, ejecting tephra, driving out magma, and causing pressure and eruption-rate surges at the vent 40 km distant. Magma pressure driving the eruption (above magmastatic) was very low between the HCR and vent. Thus, it appears that collapse-induced reservoir pressurization sustained the eruption—and therefore that the onset of caldera collapse represents a critical threshold in a large eruption sequence. Observed tephra explosions were not driven by magma-water interactions, as expected from widely accepted conceptual models, but rather primarily by vent and caldera collapse processes. This suggests a reevaluation of Kīlauea's 1924 explosions and increases the recognition that basaltic shield volcano collapses can result in hazardous explosive activity through a variety of mechanisms (other possible hazards include seismic shaking and the generation of tsunamis).

The volume and intensity of the eruption and summit collapse are reflections of the hydraulic connection between the summit and rift zone and the driving influence of caldera collapse. The eruption illustrated a magmatic-tectonic system that is tightly interconnected, with (often cyclic) complex feedback mechanisms and consequently interrelated hazards over tens of kilometers and

over timescales spanning minutes to decades. The rate of magma supply to Kīlauea during the eruption was roughly two orders of magnitude lower than the eruption rate and did not control the evolution of the eruption. Rather, both summit- and rift-driven processes including caldera collapse, changes in rift zone magma viscosity, and the evolving intrusion geometry played important governing roles. Although details of the physical connection between summit magma reservoirs and the rift zone remain ambiguous, it is likely more complex than previously envisioned.

Kīlauea's 2018 eruption was driven by a complex mix of cascading physical processes, but gravity played a particularly important role, affecting many parts of the volcano: in long-term stress accumulation on the décollement, as potential energy (magmatic head) between the summit and rift zone, and in subsidence of the caldera blocks that drove the eruption. The potential energy driving these processes was supplied by the ascent of magma into the volcano over previous decades and centuries. Eruptions like the one in 2018 rebalance the system, converting potential energy into décollement slip, rift zone opening, and movement of magma tens of kilometers from the summit.

Extensive draining of the magma system revealed in new detail magma stored in numerous parts of the volcano in diverse volumes and compositions. At the summit, the caldera collapsed into several cubic kilometers of compressible magma stored at shallow depth, revealing its geometry and volume as never before. Magma storage bodies in the ERZ are larger and contain more potentially mobile magma than generally understood, and their existence adds to evidence that silicic magmas may be common at basaltic volcanoes (e.g., Wieser et al. 2022) and play an important role in controlling eruption rate and hazard, in part through their influence on the composition of erupted lava.

The 2018 eruption confirms and further elucidates ideas about how shield volcanoes like Kīlauea grow and evolve. Despite its historical significance, the eruption was much smaller than caldera-forming collapses that have heralded transitions to dominantly explosive eras of volcanism at the volcano in past centuries. Eruptions similar to that in 2018 have happened numerous times in Kīlauea's past and will happen again.

In many ways, the 2018 collapse was remarkably similar to historical collapses at other basaltic volcanoes, including triggering by low-elevation rift zone intrusions (some, as at Bárdarbunga, also propagating tens of kilometers) and cycles of abrupt summit collapse accompanied by inflationary ground deformation and release of VLP seismic energy (e.g., Michon et al. 2011, Gudmundsson et al. 2016). A pattern begins to emerge of a class of eruptions more common than previously recognized (e.g., Sigmundsson 2019) in which sublateral magma flow to low elevations efficiently drains summit reservoirs, triggering episodic caldera collapse, which in turn drives magma outflow, sustaining eruptions. Because these kinds of eruptions can efficiently move large volumes of magma large distances in relatively short periods of time, they represent a significant hazard even tens of kilometers from volcanic summits (Sigmundsson 2019).

4.2. Open Questions and Avenues for Future Work

Here we present 10 open questions that we view as particularly important and, we hope, amenable to future progress. New questions will arise with further work, and many new mysteries presumably await.

1. Did changes in magma supply rate (MSR) precede and/or follow the 2018 eruption, and if so, what was the causal mechanism? The possibility of an increase in MSR remains circumstantial but intriguing (see, for instance, the rate of Pāhala earthquakes in Figure 3a) and could portend a more active system in the future. Resolving changes in MSR may improve our understanding of the governing physical controls and, perhaps, magma supply paths (e.g., Dvorak &

1 28 Anderson et al.



- Dzurisin 1993). Efforts to better understand the relation between MSR and potential proxy observations such as earthquake rates, high-Fo olivine, ³He/⁴He ratios, and CO₂ emissions (currently not well constrained at Kīlauea) are warranted; MSR may also be constrained using post-2018 geodetic and eruption rate data together with mass-balance models.
- 2. What is the role of décollement earthquakes in promoting rift opening, large eruptions, and summit collapses? Historically, rift zone intrusions and summit draining events have often—but not always—been closely associated with flank slip events. How (or even if) the 2018 ~Mw7 earthquake facilitated magma transport and/or storage in the rift zone, sustaining the eruption and promoting collapse, remains unclear. Analysis of historical eruptions may prove illustrative, better elucidating the complex interactions that appear to give rise to quasiperiodic magmatic-tectonic cycles at Kīlauea, and helping to resolve the roles of magma supply, magma pressure, gravity, and even stress imparted by neighboring Mauna Loa. Clues may also be found at other global rift zone volcanoes, some of which similarly show strongly correlated magma-flank interactions (e.g., Krafla and Etna), and some of which do not (e.g., Ambrym).
- 3. How do basaltic calderas collapse, and what are the inferences for magma storage and nonvolcanic earthquakes? Observations of episodic collapse at Kīlauea are surprisingly consistent with simple models, yet the growth and geometrical complexity of faulting throughout the collapse sequence (including its influence on geophysical data), the role of preexisting geologic structures and heterogeneous fault properties, slip nucleation and acceleration, inelastic deformation of the subsiding blocks, creeping intercollapse subsidence, and the interaction between the subsiding roof blocks and the magma reservoir are all only crudely understood. Detailed analysis of extensive visual imagery should resolve the morphological evolution of the caldera in detail, permitting comparison with subsurface processes as inferred from geophysical data. Collapse models utilizing particle-based approaches (e.g., Holohan et al. 2015, Mullet et al. 2023) or three-dimensional dynamic and quasi-dynamic rupture and collapse cycle simulations may predict the spatiotemporal evolution of fault slip and reservoir pressure. These models may be related with seismic waveforms and high-rate geodetic data, yielding insight into faulting, subcaldera magma storage, and the internal structural evolution of the caldera. Comparing Kīlauea with other basaltic collapses will help separate universal driving physics from volcano-specific geometries and material properties. Progress should improve scientists' ability to understand and forecast the onset and evolution of caldera collapses, while insights into fault friction and earthquake mechanics should have important implications for understanding nonvolcanic earthquakes as well.
- 4. How can lessons from the 2018 collapse be applied to other eruptions? The conditions under which caldera collapses begin and evolve are influenced by myriad factors including the physical properties of the subcaldera magma system (e.g., maturity, compressibility, geometry) and the roof rock (e.g., preexisting structures). These conditions can vary greatly between volcanoes and even over time at the same volcano, so it is perhaps surprising that all (or nearly all) historical basaltic caldera collapses evolved episodically rather than continuously. Comparison with past events at Kīlauea—furthered by new studies to better elucidate collapse (lowering) cycles over Kīlauea's past 2,500 years—will be useful to ascertain, for instance, why summit collapses have been more frequent during some periods, and why low-elevation LERZ intrusions and eruptions in 1955 and 1960 did not result in major summit failure [tectonic effects (question 2) and Kīlauea's 2008–2018 lava lake were likely important]. Finally, an important long-term goal will be to determine how lessons learned from basaltic collapses may or may not be applied to explosive silicic caldera-forming eruptions, which can be some of Earth's most hazardous natural phenomena.

- 5. How complex is the geometry of magma storage beneath Kīlauea's summit, and how does magma enter the ERZ? Our conception of Kīlauea's summit magma storage system is shaped in part by reliance on geometrically simple deformation and seismic source models, the limitations of which have been highlighted by the remarkable data collected in 2018. The basic physical properties of the SCR remain unclear, along with the reservoir's role in triggering and supplying the 2018 eruption. Furthermore, the physical connections between the summit storage reservoirs and the ERZ remain one of the great outstanding questions of Kīlauea's magma plumbing system. We expect many new insights in the coming years through the development of geodetic models and physics-based magma flow models that utilize the different spatiotemporal deformation patterns of the two reservoirs, include more complex source geometries, and couple magma withdrawal with rift zone magma flow and eruption. Improved characterization of ERZ magma surges may also elucidate details of summit-rift zone connectivity as well as flow in the rift zone (next question).
- 6. How does magma accumulate and flow in the rift zones? The mechanisms and durations over which magma storage zones in the ERZ form and fail (permitting downrift flow); their compositions and physical characteristics, volumes, depths (including the possibility of storage in the deep rift); and their relation to the long-lived eruption at Pu'u'ō'ō all remain unclear. The delay between the Pu'u'ō'ō collapse and onset of summit deflation, the delay between caldera collapse events and eruption surges, and draining and subsequent refilling of the MERZ offer many clues into rift zone storage geometries and physical properties (e.g., melt fractions). Changes in deformation rates should also help to separate the role of magmatic and gravitational forces in flank slip, and an improved post-2018 monitoring network may better detect any magma flow into the LERZ. Models based on the physics of magma flow—including those that account for the porous flow of magma through a crystal mush—can utilize diverse observations and be used to constrain volumes, physical properties, and connectivities.
- 7. How were summit explosions produced by caldera collapse? Tephra emissions are common during basaltic collapses, and explosive activity is common at Kīlauea—yet closely observed explosions at shield volcanoes are rare. The 2018 eruption yielded a rich library of plume photos and videos that remains largely untapped, together with weather radar data, related geophysical signals, and tephra samples. These observations have only begun to be exploited and may shed light on the shallow magma system, the mechanisms by which caldera collapses explosively eject tephra, and contribute more generally to efforts to model volcanic tephra plumes.
- 8. How did summit-driven and rift-driven processes interact to control and ultimately end the eruption? The physical mechanisms relating changes in caldera collapse with changes in the LERZ eruption (magma composition and eruption rates) are not understood. Furthermore, despite abundant monitoring data, the end of the 2018 eruption was unexpected. A careful search for subtle changes in monitoring data—such as the geophysical signals produced by the repetitive summit collapse events—may yet reveal precursory changes. An improved understanding of the role of the SCR in driving the eruption is also required (question 5) in order to fully understand its end.
- 9. How did the 2018 eruption change Kīlauea, and how do Hawaiian volcanoes interact with one another? The long-term effects of the 2018 eruption are not yet clear and could conceivably include increases in MSR, changes in flank tectonics, and changes in rift zone magma storage and downrift flow in the post-Pu'u'ō'ō ERZ (a related question is when and where eruptions will once again resume in the ERZ). It also remains unclear how 2018 may have manifested on other major structures at Kīlauea, such as the SWRZ. Hazard managers will also need

1.30 Anderson et al.



- to contend with the possibility of a more active Mauna Loa, which experienced heightened unrest following 2018 and erupted in 2022 after a 38-year repose. Efforts to resolve any changes before they manifest as eruptive activity are important for providing actionable hazard forecasts and should help better resolve the physical processes by which Hawai'i's volcanoes and geologic structures are coupled.
- 10. Can large caldera-rift eruptions and associated hazards be effectively forecast? Ultimately, a primary goal of volcanology is to forecast the onset, style, duration, and volume of eruptions. In 2018, volcanologists correctly anticipated a change in the ongoing Pu'u'ō'ō eruption but not the scale of subsequent events, despite observations of similar past activity at Kīlauea and other basaltic volcanoes. Connecting short-term monitoring data with insights from long-term activity and from global eruptions is thus a challenge, as is anticipating the complex cascading physical processes that may occur during an eruption. Nonetheless, improved understanding of Kīlauea's magmatic-tectonic system hints at a future in which models and monitoring data are coupled to track the stress state of the volcano's flanks together with changes in magma pressure that push the system toward failure, yielding an evolving probabilistic assessment of hazard. Improved understanding of periodicity in magmatic-tectonic activity, changes in MSR, silent magma injection into the rift zones, and the role of longlived MERZ eruptions in promoting rift failure would improve these efforts. Improved caldera collapse models may also someday be employed to track an evolving collapse sequence, foretelling individual collapse events and/or the cessation of the eruption. Finally, while volcanologists had success in 2018 assessing and forecasting hazards using a variety of methods, including expert elicitation and lava flow models, much more work is needed to improve our ability to quantitatively forecast possible hazards during large rift-caldera eruptions, including those from related hazards such as ground shaking and tsunamis. The 2018 eruption also reinforced the challenges associated with quantifying and communicating uncertainties in these potential outcomes to the public, suggesting new efforts at the interface of volcanology, statistics, and communications.

4.3. Final Thoughts

The 2018 eruption of Kīlauea Volcano offered an unprecedented opportunity to witness and study volcanic processes occurring in concert along a 40-km-long volcanic segment, elucidating in remarkable detail processes that occur widely at Earth's volcanoes. This watershed event will have an outsized influence on our understanding of global basaltic volcanism and associated hazards.

Nonetheless, Kīlauea's 2018 eruption was but one of several recent basaltic eruptions of consequence. These include rift-driven basaltic caldera collapses at Miyakejima, Piton de la Fournaise, and Bárdarbunga (Nakada et al. 2005, Michon et al. 2007, Gudmundsson et al. 2016); intrusions and lava lake drainage at Ambrym and Nyiragongo (Shreve et al. 2019, Smittarello et al. 2022); and months-long eruptions at Fagradalsfjall and La Palma, which, as at Kīlauea, permitted the implementation of numerous observational techniques (Bindeman et al. 2022, Wadsworth et al. 2022). Together, these eruptions have substantially improved understanding of basaltic volcanism.

Kīlauea's 2018 eruption inspired efforts to improve the institutional capacity of the USGS to respond to major volcanic eruptions (Williams et al. 2020), contributed to improved communications within the volcanological community, and brought new resources to bear on understanding the volcano. The National Science Foundation (NSF)-funded CONVERSE initiative arose in part from the 2018 eruption to better coordinate critical data collection efforts and maximize scientific returns during eruptions (Fischer et al. 2021), and has already borne fruit during several



post-2018 Hawaiian eruptions (Cooper et al. 2023). The US Congress also allocated disaster supplemental funding to enhance monitoring of Hawaiian volcanoes and support new research projects. These efforts should help to usher in a new era of cooperative volcanology at Kīlauea and other volcanoes.

The basic conceptual model of Kīlauea—developed and refined over more than a century of intensive research into Hawaiian volcanism (e.g., Eaton & Murata 1960, Tilling & Dvorak 1993, Ryan 1988, Poland et al. 2014)—stood up remarkably well to the test of 2018. Indeed, it is perhaps surprising how unsurprising the 2018 eruption was in many ways. Yet, volcanological puzzles abound, a wealth of observational data remain largely untapped, and a new generation of sophisticated models are only beginning to be developed and employed. We expect that many of the scientific conclusions presented in this review will require extensive revision by work conducted in the coming years.

Finally, although the 2018 eruption of Kīlauea was exceptionally well documented by historical standards, similarly detailed observations are likely to become increasingly common during future eruptions around the world. In this sense, the 2018 eruption may herald a new era of volcanology in which eruptions are recorded in a wide variety of local and remote field, geophysical, and petrological data sets. These observations should support a new generation of detailed analysis and modeling efforts but will require interdisciplinary scientific coordination across disciplines, institutes, and international boundaries. We anticipate that well-recorded eruptions, such as at Kīlauea in 2018, will motivate enduring collaborations that leverage collective skills of the broader science community, driving leaps in our ability to understand volcanic systems and forecast hazards throughout the twenty-first century.

DISCLOSURE STATEMENT

The authors are not aware of any affiliations, memberships, funding, or financial holdings that might be perceived as affecting the objectivity of this review.

ACKNOWLEDGMENTS

We are indebted to colleagues too numerous to list here for eruption response efforts and for discussions that benefited this work. Hawai'i Volcanoes National Park supported monitoring networks and campaign instrumentation during the response. Some of the studies described in this work were supported by the Additional Supplemental Appropriations for Disaster Relief Act of 2019 (P.L. 116-20). T.S. acknowledges National Science Foundation Division of Earth Sciences grant 2020045. Any use of trade, firm, or product names is for descriptive purposes only and does not imply endorsement by the US government.

LITERATURE CITED

Anderson K, Johanson I. 2022. Incremental caldera collapse at Kīlauea Volcano recorded in ground tilt and high-rate GNSS data, with implications for collapse dynamics and the magma system. Bull. Volcanol. 84:89 Anderson KR, Johanson IA, Patrick MR, Gu M, Segall P, et al. 2019. Magma reservoir failure and the onset of caldera collapse at Kīlauea Volcano in 2018. Science 366(6470):eaaz1822

Anderson KR, Poland MP, Johnson JH, Miklius A. 2015. Episodic deflation-inflation events at Kīlauea Volcano and implications for the shallow magma system. In Hawaiian Volcanoes: From Source to Surface, ed. R Carey, V Cayol, M Poland, D Weis, pp. 229–50. Hoboken, NJ: Wiley & Sons

Ando M. 1979. The Hawaii earthquake of November 29, 1975: low dip angle faulting due to forceful injection of magma. J. Geophys. Res. 84(B13):7616-26

Bai Y, Ye L, Yamazaki Y, Lay T, Cheung KF. 2018. The 4 May 2018 M_w 6.9 Hawaii island earthquake and implications for tsunami hazards. Geophys. Res. Lett. 45(20):11040-49

Anderson et al. I.32



- Baker S, Amelung F. 2012. Top-down inflation and deflation at the summit of Kīlauea Volcano, Hawai'i observed with InSAR. J. Geophys. Res. 117(B12):B12406
- Bindeman IN, Deegan FM, Troll VR, Thordarson T, Höskuldsson Á, et al. 2022. Diverse mantle components with invariant oxygen isotopes in the 2021 Fagradalsfjall eruption, Iceland. *Nat. Commun.* 13(1):3737
- Burgess MK, Roman DC. 2021. Ongoing (2015–) magma surge in the upper mantle beneath the island of Hawai'i. *Geophys. Res. Lett.* 48(7):e2020GL091096
- Cahalan R, Mastin LG, Van Eaton AR, Hurwitz S, Smith AB, et al. 2023. Dynamics of the December 2020 ash-poor plume formed by lava-water interaction at the summit of Kīlauea Volcano, Hawaiʻi. *Geochem. Geophys. Geosyst.* 24(3):e2022GC010718
- Carey RJ, Manga M, Degruyter W, Swanson D, Houghton B, et al. 2012. Externally triggered renewed bubble nucleation in basaltic magma: the 12 October 2008 eruption at Halema'uma'u Overlook vent, Kīlauea, Hawai'i, USA. J. Geophys. Res. 117(B11):B11202
- Cashman KV, Mangan MT. 2014. A century of studying effusive eruptions in Hawai'i. In Characteristics of Hawaiian Volcanoes, ed. MP Poland, TJ Takahashi, CM Landowski, pp. 357–94. Reston, VA: US Geol. Surv
- Cayol V, Dieterich JH, Okamura AT, Miklius A. 2000. High magma storage rates before the 1983 eruption of Kilauea, Hawaii. Science 288(5475):2343–46
- Cervelli PF, Miklius A. 2003. The shallow magmatic system of Kilauea Volcano. In *The Pu'u 'Ö'ö Küpaianaha Eruption of Kilauea Volcano, Hawai'i: The First 20 Years*, ed. C Heliker, DA Swanson, TJ Takahashi, pp. 149–64. Reston, VA: US Geol. Surv.
- Chen K, Smith JD, Avouac J, Liu Z, Song YT, Gualandi A. 2019. Triggering of the Mw 7.2 Hawaii earthquake of 4 May 2018 by a dike intrusion. *Geophys. Res. Lett.* 46(5):2503–10
- Clague DA, Denlinger RP. 1994. Role of olivine cumulates in destabilizing the flanks of Hawaiian volcanoes. Bull. Volcanol. 56(6-7):425-34
- Cooper KM, Anderson K, Cashman K, Coombs M, Dietterich H, et al. 2023. Coordinating science during an eruption: lessons from the 2020–2021 Kīlauea volcanic eruption. *Bull. Volcanol.* 85(5):29
- Crozier J, Karlstrom L. 2021. Wavelet-based characterization of very-long-period seismicity reveals temporal evolution of shallow magma system over the 2008–2018 eruption of Kīlauea Volcano. *J. Geophys. Res. Solid Earth* 126:e2020JB020837
- Crozier J, Karlstrom L. 2022. Evolving magma temperature and volatile contents over the 2008–2018 summit eruption of Kīlauea Volcano. *Sci. Adv.* 8(22):eabm4310
- Crozier JA, Karlstrom L, Dufek J, Anderson KR, Thelen WA, et al. 2018. Hindcasting May 2018 Kilauea summit explosions with remote sensing, geophysical monitoring, and eruption simulations. Part 1: seismic source inversions and self-consistent initial conditions for plume models. *AGU Fall Meet. Abstr.* 2018:V43J–0274
- Cui X, Li Z, Huang H. 2021. Subdivision of seismicity beneath the summit region of Kilauea volcano: implications for the preparation process of the 2018 eruption. *Geophys. Res. Lett.* 48(20):e2021GL094698
- Dawson P, Chouet B. 2014. Characterization of very-long-period seismicity accompanying summit activity at Kīlauea Volcano, Hawai'i: 2007–2013. 7. Volcanol. Geotherm. Res. 278–279:59–85
- deGraffenried R, Hammer J, Dietterich H, Perroy R, Patrick M, Shea T. 2021. Evaluating lava flow propagation models with a case study from the 2018 eruption of Kīlauea Volcano, Hawai'i. *Bull. Volcanol.* 83(11):65
- Delaney PT, Fiske RS, Miklius A, Okamura AT, Sako MK. 1990. Deep magma body beneath the summit and rift zones of Kilauea Volcano, Hawaii. *Science* 247(4948):1311–16
- Denlinger RP. 2019. Anatomy of Kilauea volcano. AGU Fall Meet. Abstr. 2019:V51A-06
- Denlinger RP, Flinders A. 2022. Density structure of the island of Hawai'i and the implications for gravity-driven motion of the south flank of Kīlauea Volcano. *Geophys. J. Int.* 228(3):1793–807
- Denlinger RP, Morgan JK. 2014. Instability of Hawaiian volcanoes. In *Characteristics of Hawaiian Volcanoes*, ed. MP Poland, TJ Takahashi, CM Landowski, pp. 149–76. Reston, VA: US Geol. Surv.
- Dieterich JH. 1988. Growth and persistence of Hawaiian volcanic rift zones. *J. Geophys. Res.* 93(B5):4258–70 Dieterich HR, Diefenbach AK, Soule SA, Zoeller MH, Patrick MP, et al. 2021. Lava effusion rate evolution and erupted volume during the 2018 Kīlauea lower East Rift Zone eruption. *Bull. Volcanol.* 83(4):25



- Dietterich HR, Grant GE, Fasth B, Major JJ, Cashman KV. 2022. Can lava flow like water? Assessing applications of critical flow theory to channelized basaltic lava flows. J. Geophys. Res. Earth Surface 127:e2022JF006666
- Druitt TH, Sparks RSJ. 1984. On the formation of calderas during ignimbrite eruptions. Nature 310(5979):679-81
- Dvorak JJ, Dzurisin D. 1993. Variations in magma supply rate at Kilauea Volcano, Hawaii. 7. Geophys. Res. 98(B12):22255-68
- Eaton JP, Murata KJ. 1960. How volcanoes grow: Geology, geochemistry, and geophysics disclose the constitution and eruption mechanism of Hawaiian volcanoes. Science 132(3432):925-38
- Elias T, Kern C, Horton KA, Sutton AJ, Garbeil H. 2018. Measuring SO₂ emission rates at Kīlauea Volcano, Hawaii, using an array of upward-looking UV spectrometers, 2014-2017. Front. Earth Sci. 6:214
- Epp D, Decker RW, Okamura AT. 1983. Relation of summit deformation to East Rift Zone eruptions on Kilauea Volcano, Hawaii. Geophys. Res. Lett. 10(7):493-96
- Farquharson JI, Amelung F. 2020. Extreme rainfall triggered the 2018 rift eruption at Kīlauea Volcano. Nature 580(7804):491-95
- Feng KF, Huang HH, Wu YM. 2020. Detecting pre-eruptive magmatic processes of the 2018 eruption at Kilauea, Hawaii volcano with ambient noise interferometry. Earth Planets Space 72(1):74
- Fischer T, Moran S, Cooper K, Roman D, LaFemina P. 2021. Making the most of volcanic eruption responses. Eos 102. https://doi.org/10.1029/2021EO162790
- Fiske RS, Rose TR, Swanson DA, Andrews BJ, Nichols AR. 2019. The Kulanaokuaiki-3 tephra, 900 CE: products of a remarkably energetic pyroclastic eruption at Kīlauea Volcano, Hawai'i, USA. Geol. Soc. Am. Bull. 131(9-10):1537-54
- Flinders AF, Caudron C, Johanson IA, Taira T, Shiro B, Haney M. 2020a. Seismic velocity variations associated with the 2018 lower East Rift Zone eruption of Kīlauea, Hawai'i. Bull. Volcanol. 82(6):47
- Flinders AF, Johanson IA, Dawson PB, Anderson KR, Haney MM, Shiro BR. 2020b. Very-long-period (VLP) seismic artifacts during the 2018 caldera collapse at Kīlauea, Hawai'i. Seismol. Res. Lett. 91(6):3417-32
- Gansecki C, Lee RL, Shea T, Lundblad SP, Hon K, Parcheta C. 2019. The tangled tale of Kīlauea's 2018 eruption as told by geochemical monitoring. Science 366(6470):eaaz0147
- Garcia MO. 2015. How and why Hawaiian volcanism has become pivotal to our understanding of volcanoes from their source to the surface. In Hawaiian Volcanoes: From Source to Surface, ed. R Carey, V Cayol, M Poland, D Weis, pp. 1-18. Hoboken, NJ: Wiley & Sons
- Garcia MO, Pietruszka AJ, Norman MD, Rhodes JM. 2021. Kīlauea's Pu'u'Ō'ō eruption (1983-2018): a synthesis of magmatic processes during a prolonged basaltic event. Chem. Geol. 581:120391
- Gudmundsson A. 2015. Collapse-driven large eruptions. J. Volcanol. Geotherm. Res. 304:1-10
- Gudmundsson MT, Jónsdóttir K, Hooper A, Holohan EP, Halldórsson SA, et al. 2016. Gradual caldera collapse at Bárdarbunga volcano, Iceland, regulated by lateral magma outflow. Science 353(6296):aaf8988
- Haney MM, Patrick MR, Anderson KR. 2016. Ground tilt time delays between Kīlauea Volcano's summit and East Rift Zone caused by magma reservoir buffering. AGU Fall Meet. Abstr. 2016:V12A-06
- Heliker C, Mattox TN. 2003. The first two decades of the Pu'u 'Ö'ö-Küpaianaha eruption: chronology and selected bibliography. In The Pu'u 'Ö'ö-Küpaianaha Eruption of Kilauea Volcano, Hawai'i: The First 20 Years, ed. C Heliker, DA Swanson, TJ Takahashi, pp. 1-28. Reston, VA: US Geol. Surv.
- Helz RT, Thornber CR. 1987. Geothermometry of Kilauea Iki lava lake, Hawaii. Bull. Volcanol. 49(5):651-68
- Helz RT, Wright TL. 1992. Differentiation and magma mixing on Kilauea's east rift zone: a further look at the eruptions of 1955 and 1960. Part I. The late 1955 lavas. Bull. Volcanol. 54(5):361-84
- Hill DP, Zucca JJ. 1987. Geophysical constraints on the structure of Kilauea and Mauna Loa Volcanoes and some implications for seismomagmatic processes. In Volcanism in Hawaii, ed. RW Decker, TL Wright, PH Stauffer, pp. 903–17. Washington, DC: US Geol. Surv.
- Holcomb RT. 1987. Eruptive history and long-term behavior of Kilauea Volcano. In Volcanism in Hawaii, ed. RW Decker, TL Wright, PH Stauffer, pp. 261-350. Washington, DC: US Geol. Surv.
- Holohan E, Schöpfer M, Walsh J. 2015. Stress evolution during caldera collapse. Earth Planet. Sci. Lett. 421:139-51

Anderson et al. I.34



- Hotovec-Ellis AJ, Shiro BR, Shelly DR, Anderson KR, Haney MM, et al. 2022. Earthquake-derived seismic velocity changes during the 2018 caldera collapse of Kīlauea Volcano. J. Geophys. Res. Solid Earth 127:e2021JB023324
- Houghton B, Swanson D, Carey R, Rausch J, Sutton A. 2011. Pigeonholing pyroclasts: insights from the 19 March 2008 explosive eruption of Kīlauea volcano. Geology 39(3):263-66
- Houghton BF, Tisdale CM, Llewellin EW, Taddeucci J, Orr TR, et al. 2021. The birth of a Hawaiian fissure eruption. J. Geophys. Res. Solid Earth 126:e2020JB020903
- Hsieh PA, Ingebritsen SE. 2019. Groundwater inflow toward a preheated volcanic conduit: application to the 2018 eruption at Kīlauea Volcano, Hawai'i. J. Geophys. Res. Solid Earth 124:1498-506
- James M, Carr B, D'Arcy F, Diefenbach A, Dietterich H, et al. 2020. Volcanological applications of unoccupied aircraft systems (UAS): developments, strategies, and future challenges. Volcanica 3(1):67-114
- Johnson DJ. 1995. Molten core model for Hawaiian rift zones. J. Volcanol. Geotherm. Res. 66(1-4):27-35
- Kehoe HL, Kiser ED, Okubo PG. 2019. The rupture process of the 2018 M_w 6.9 Hawai'i earthquake as imaged by a genetic algorithm-based back-projection technique. Geophys. Res. Lett. 46(5):2467-74
- Kern C, Lerner AH, Elias T, Nadeau PA, Holland L, et al. 2020. Quantifying gas emissions associated with the 2018 rift eruption of Kīlauea Volcano using ground-based DOAS measurements. Bull. Volcanol. 82(7):55
- Kumagai H, Ohminato T, Nakano M, Ooi M, Kubo A, et al. 2001. Very-long-period seismic signals and caldera formation at Miyake Island, Japan. Science 293(5530):687-90
- Kundu B, Yadav RK, Bürgmann R, Wang K, Panda D, Gahalaut VK. 2020. Triggering relationships between magmatic and faulting processes in the May 2018 eruptive sequence at Kīlauea volcano, Hawaii. Geophys. J. Int. 222(1):461-73
- Lai VH, Zhan Z, Brissaud Q, Sandanbata O, Miller MS. 2021. Inflation and asymmetric collapse at Kīlauea summit during the 2018 eruption from seismic and infrasound analyses. 7. Geophys. Res. Solid Earth 126:e2021JB022139
- Lay T, Ye L, Kanamori H, Satake K. 2018. Constraining the dip of shallow, shallowly dipping thrust events using long-period Love wave radiation patterns: applications to the 25 October 2010 Mentawai, Indonesia, and 4 May 2018 Hawaii Island earthquakes. Geophys. Res. Lett. 45(19):10342-49
- Lengliné O, Duputel Z, Okubo P. 2021. Tracking dike propagation leading to the 2018 Kīlauea eruption. Earth Planet. Sci. Lett. 553:116653
- Lerner AH, Wallace PJ, Shea T, Mourey AJ, Kelly PJ, et al. 2021. The petrologic and degassing behavior of sulfur and other magmatic volatiles from the 2018 eruption of Kīlauea, Hawai'i: melt concentrations, magma storage depths, and magma recycling. Bull. Volcanol. 83(6):43
- Liang C, Dunham EM. 2020. Lava lake sloshing modes during the 2018 Kīlauea Volcano eruption probe magma reservoir storativity. Earth Planet. Sci. Lett. 535:116110
- Lin G, Shearer PM. 2021. Spatiotemporal variations of focal mechanism and in situ Vp/Vs ratio during the 2018 Kīlauea eruption. Geophys. Res. Lett. 48(18):e2021GL094636
- Lin JT, Aslam KS, Thomas AM, Melgar D. 2020. Overlapping regions of coseismic and transient slow slip on the Hawaiian décollement. Earth Planet. Sci. Lett. 544:116353
- Liu C, Lay T, Xiong X. 2018. Rupture in the 4 May 2018 M_W 6.9 earthquake seaward of the Kilauea East Rift Zone fissure eruption in Hawaii. Geophys. Res. Lett. 45(18):9508-15
- Lundgren P, Bagnardi M, Dietterich H. 2019. Topographic changes during the 2018 Kīlauea eruption from single-pass airborne InSAR. Geophys. Res. Lett. 46(16):9554-62
- Lynn KJ. 2022. Olivine and glass analyses for select eruptions of Kilauea Volcano, Hawai'i. Data release: US Geol. Surv., Reston, VA. https://doi.org/10.5066/P9HA3PRK
- Lynn KJ, Shea T, Garcia MO. 2017. Nickel variability in Hawaiian olivine: evaluating the relative contributions from mantle and crustal processes. Am. Mineral. 102(3):507-18
- Lynn KJ, Swanson DA. 2022. Olivine and glass chemistry record cycles of plumbing system recovery after summit collapse events at Kīlauea Volcano, Hawai'i. J. Volcanol. Geotherm. Res. 426:107540
- Lyons JJ, Dietterich HR, Patrick MP, Fee D. 2021. High-speed lava flow infrasound from Kīlauea's fissure 8 and its utility in monitoring effusion rate. Bull. Volcanol. 83(11):66
- Mastin LG, Christiansen RL, Swanson DA, Stauffer PH, Hendley JWI. 1999. Explosive eruptions at Kilauea Volcano, Hawai'i? Fact Sheet 132-98, US Geol. Surv., Reston, VA. https://doi.org/10.3133/fs13298



- McMurtry GM, Dasilveira LA, Horn EL, DeLuze JR, Blessing JE. 2019. High ³He/⁴He ratios in lower East Rift Zone steaming vents precede a new phase of Kilauea 2018 eruption by 8 months. Sci. Rep. 9(1):11860
- Michon L, Massin F, Famin V, Ferrazzini V, Roult G. 2011. Basaltic calderas: collapse dynamics, edifice deformation, and variations of magma withdrawal. J. Geophys. Res. 116(B3):B03209
- Michon L, Staudacher T, Ferrazzini V, Bachèlery P, Marti J. 2007. April 2007 collapse of Piton de la Fournaise: a new example of caldera formation. Geophys. Res. Lett. 34(21):L21301
- Michon L, Villeneuve N, Catry T, Merle O. 2009. How summit calderas collapse on basaltic volcanoes: new insights from the April 2007 caldera collapse of Piton de la Fournaise volcano. J. Volcanol. Geotherm. Res. 184(1-2):138-51
- Montagna CP, Gonnermann HM. 2013. Magma flow between summit and Pu'u 'O'ō at Kīlauea Volcano, Hawai'i. Geochem. Geophys. Geosyst. 14(7):2232-46
- Montgomery-Brown EK, Miklius A. 2020. Periodic dike intrusions at Kīlauea volcano, Hawai'i. Geology 49(4):397-401
- Montgomery-Brown EK, Poland MP, Miklius A. 2015. Delicate balance of magmatic-tectonic interaction at Kīlauea Volcano, Hawai'i, revealed from slow slip events. In Hawaiian Volcanoes: From Source to Surface, ed. R Carey, V Cayol, M Poland, D Weis, pp. 269-88. Hoboken, NJ: Wiley & Sons
- Mourey AJ, Shea T, Costa F, Shiro B, Longman RJ. 2023a. Years of magma intrusion primed Kīlauea Volcano (Hawai'i) for the 2018 eruption: evidence from olivine diffusion chronometry and monitoring data. Bull. Volcanol. 85(3):18
- Mourey AJ, Shea T, Hammer JE. 2023b. Preservation of magma recharge signatures in Kīlauea olivine during protracted storage. 7. Geophys. Res. Solid Earth 128(1):e2022JB025523
- Mourey AJ, Shea T, Lynn KJ, Lerner AH, Lambart S, et al. 2022. Trace elements in olivine fingerprint the source of 2018 magmas and shed light on explosive-effusive eruption cycles at Kīlauea Volcano. Earth Planet. Sci. Lett. 595:117769
- Mullet B, Segall P, Fávero Neto AH. 2023. Numerical modeling of caldera formation using smoothed particle hydrodynamics (SPH). Geophys. 7. Int. 234(2):887–902
- Nakada S, Nagai M, Kaneko T, Nozawa A, Suzuki-Kamata K. 2005. Chronology and products of the 2000 eruption of Miyakejima Volcano, Japan. Bull. Volcanol. 67(3):205-18
- Namiki A, Patrick MR, Manga M, Houghton BF. 2021. Brittle fragmentation by rapid gas separation in a Hawaiian fountain. Nat. Geosci. 14(4):242-47
- Neal CA, Anderson KR. 2020. Preliminary analyses of volcanic hazards at Kīlauea Volcano, Hawai'i, 2017-2018. Open File Rep. 2020-1002, US Geol. Surv., Reston, VA. https://doi.org/10.3133/ofr20201002
- Neal CA, Brantley SR, Antolik L, Babb JL, Burgess M, et al. 2019. The 2018 rift eruption and summit collapse of Kīlauea Volcano. Science 363(6425):367-74
- Olivier G, Brenguier F, Carey R, Okubo P, Donaldson C. 2019. Decrease in seismic velocity observed prior to the 2018 eruption of Kīlauea Volcano with ambient seismic noise interferometry. Geophys. Res. Lett. 46(7):3734-44
- Orr TR, Poland MP, Patrick MR, Thelen WA, Sutton AJ, et al. 2015. Kīlauea's 5-9 March 2011 Kamoamoa fissure eruption and its relation to 30+ years of activity from Pu'u 'O'ō. In Hawaiian Volcanoes: From Source to Surface, ed. R Carey, V Cayol, M Poland, D Weis, pp. 393-420. Hoboken, NJ: Wiley & Sons
- Orr TR, Thelen WA, Patrick MR, Swanson DA, Wilson DC. 2013. Explosive eruptions triggered by rockfalls at Kīlauea volcano, Hawai'i. Geology 41(2):207-10
- Patrick M, Orr T, Anderson K, Swanson D. 2019a. Eruptions in sync: improved constraints on Kilauea Volcano's hydraulic connection. Earth Planet. Sci. Lett. 507:50-61
- Patrick M, Orr T, Swanson D, Houghton B, Wooten K, et al. 2021. Kīlauea's 2008-2018 summit lava lakechronology and eruption insights. Prof. Pap. 1867, US Geol. Surv., Reston, VA. https://doi.org/10.3133/
- Patrick M, Swanson D, Orr T. 2019b. A review of controls on lava lake level: insights from Halema'uma'u Crater, Kīlauea Volcano. Bull. Volcanol. 81(3):13
- Patrick MR, Dietterich HR, Lyons JJ, Diefenbach AK, Parcheta C, et al. 2019c. Cyclic lava effusion during the 2018 eruption of Kīlauea Volcano. Science 366(6470):eaay9070
- Patrick MR, Houghton BF, Anderson KR, Poland MP, Montgomery-Brown E, et al. 2020. The cascading origin of the 2018 Kīlauea eruption and implications for future forecasting. Nat. Commun. 11(1):5646

1.26 Anderson et al.



- Patrick MR, Younger EF, Tollett W. 2019d. Lava level and crater geometry data during the 2018 lava lake draining at Kīlauea Volcano, Hawaii. Data rel.: US Geol. Surv., Reston, VA. https://doi.org/10.5066/P9MJY24N
- Pietruszka AJ, Garcia MO, Rhodes JM. 2021. Accumulated Pu'u 'Ō'ō magma fed the voluminous 2018 rift eruption of Kīlauea Volcano: evidence from lava chemistry. *Bull. Volcanol.* 83(9):59
- Pietruszka AJ, Heaton DE, Marske JP, Garcia MO. 2015. Two magma bodies beneath the summit of Kīlauea Volcano unveiled by isotopically distinct melt deliveries from the mantle. *Earth Planet. Sci. Lett.* 413:90–100
- Piombo A, Dragoni M. 2021. Effusion rate from a volcanic conduit subject to pressure oscillations in a viscoelastic medium. J. Geophys. Res. Solid Earth 126:e2020JB020642
- Poland MP, Carbone D, Patrick MR. 2021a. Onset and evolution of Kīlauea's 2018 flank eruption and summit collapse from continuous gravity. *Earth Planet. Sci. Lett.* 567:117003
- Poland MP, de Zeeuw-van Dalfsen E, Bagnardi M, Johanson IA. 2019. Post-collapse gravity increase at the summit of Kīlauea Volcano, Hawai'i. *Geophys. Res. Lett.* 46(24):14430–39
- Poland MP, Hurwitz S, Kauahikaua JP, Montgomery-Brown EK, Anderson KR, et al. 2022. Rainfall an unlikely factor in Kīlauea's 2018 rift eruption. *Nature* 602(7895):E7–10
- Poland MP, Miklius A, Johanson IA, Anderson KR. 2021b. A decade of geodetic change at Kīlauea's summit—observations, interpretations, and unanswered questions from studies of the 2008–2018 Halema'uma'u eruption. In *The 2008–2018 Summit Lava Lake at Kīlauea Volcano*, *Hawai'i*, ed. MP Patrick, T Orr, D Swanson, B Houghton, no. 1867-G in U.S. Geological Survey Professional Paper. 29
- Poland MP, Miklius A, Montgomery-Brown EK. 2014. Magma supply, storage, and transport at shield-stage Hawaiian volcanoes. In *Characteristics of Hawaiian Volcanoes*, ed. MP Poland, TJ Takahashi, CM Landowski, pp. 179–234. Reston, VA: US Geol. Surv.
- Roman A, Lundgren P. 2021. Dynamics of large effusive eruptions driven by caldera collapse. *Nature* 592(7854):392–96
- Roman DC, Soldati A, Dingwell DB, Houghton BF, Shiro BR. 2021. Earthquakes indicated magma viscosity during Kīlauea's 2018 eruption. Nature 592(7853):237–41
- Ryan MP. 1988. The mechanics and three-dimensional internal structure of active magmatic systems: Kilauea Volcano, Hawaii. J. Geophys. Res. 93(B5):4213–48
- Segall P, Anderson K. 2021. Repeating caldera collapse events constrain fault friction at the kilometer scale. PNAS 118(30):e2101469118
- Segall P, Anderson K, Wang TA. 2022. Could Kīlauea's 2020 post caldera-forming eruption have been anticipated? *Geophys. Res. Lett.* 49(15):e2022GL099270
- Segall P, Anderson KR, Johanson I, Miklius A. 2019. Mechanics of inflationary deformation during caldera collapse: evidence from the 2018 Kīlauea eruption. Geophys. Res. Lett. 46(21):11782–89
- Segall P, Anderson KR, Pulvirenti F, Wang T, Johanson I. 2020. Caldera collapse geometry revealed by near-field GPS displacements at Kīlauea Volcano in 2018. *Geophys. Res. Lett.* 47(15):e2020GL088867
- Shelly DR, Thelen WA. 2019. Anatomy of a caldera collapse: Kīlauea 2018 summit seismicity sequence in high resolution. *Geophys. Res. Lett.* 46(24):14395–403
- Shiro BR, Zoeller MH, Kamibayashi K, Johanson IA, Parcheta C, et al. 2021. Monitoring network changes during the 2018 Kilauea Volcano eruption. Seismol. Res. Lett. 92(1):102–18
- Shreve T, Grandin R, Boichu M, Garaebiti E, Moussallam Y, et al. 2019. From prodigious volcanic degassing to caldera subsidence and quiescence at Ambrym (Vanuatu): the influence of regional tectonics. *Sci. Rep.* 9(1):18868
- Sigmundsson F. 2019. Calderas collapse as magma flows into rifts. Science 366(6470):1200-1
- Simkin T, Howard KA. 1970. Caldera collapse in the Galápagos Islands, 1968. Science 169(3944):429–37
- Smittarello D, Smets B, Barrière J, Michellier C, Oth A, et al. 2022. Precursor-free eruption triggered by edifice rupture at Nyiragongo volcano. *Nature* 609(7925):83–88
- Soldati A, Houghton B, Dingwell D. 2021. A lower bound on the rheological evolution of magmatic liquids during the 2018 Kilauea eruption. Chem. Geol. 576:120272
- Soubestre J, Chouet B, Dawson P. 2021. Sources of volcanic tremor associated with the summit caldera collapse during the 2018 east rift eruption of Kīlauea Volcano, Hawai'i. J. Geophys. Res. Solid Earth 126(6):e2020JB021572



- Soule SA, Zoeller M, Parcheta C. 2021. Submarine lava deltas of the 2018 eruption of Kīlauea volcano. Bull. Volcanol. 83(4):23
- Stearns HT. 1925. The explosive phase of Kilauea Volcano, Hawaii, in 1924. Bull. Volcanol. 2(2):193-208
- Swanson DA, Rose TR, Mucek AE, Garcia MO, Fiske RS, Mastin LG. 2014. Cycles of explosive and effusive eruptions at Kīlauea Volcano, Hawai'i. Geology 42(7):631-34
- Tepp G. 2021. Material failure and caldera collapse: insights from the 2018 Kilauea eruption. Earth Planet. Sci. Lett. 553:116621
- Tepp G, Hotovec-Ellis A, Shiro B, Johanson I, Thelen W, Haney MM. 2020. Seismic and geodetic progression of the 2018 summit caldera collapse of Kīlauea volcano. Earth Planet. Sci. Lett. 540:116250
- Thelen W, Waite G, Lyons J, Fee D. 2022. Infrasound observations and constraints on the 2018 eruption of Kīlauea Volcano, Hawaii. Bull. Volcanol. 84(8):76
- Thornber CR, Orr TR, Heliker C, Hoblitt RP. 2015. Petrologic testament to changes in shallow magma storage and transport during 30+ years of recharge and eruption at Kīlauea Volcano, Hawai'i. In Hawaiian Volcanoes: From Source to Surface, ed. R Carey, V Cayol, M Poland, D Weis, pp. 147-88. Hoboken, NJ: Wiley & Sons
- Tilling RI, Dvorak JJ. 1993. Anatomy of a basaltic volcano. Nature 363(6425):125-33
- Tilling RI, Kauahikaua JP, Brantley SR, Neal CA. 2014. The Hawaiian Volcano Observatory: a natural laboratory for studying basaltic volcanism. In Characteristics of Hawaiian Volcanoes, ed. MP Poland, TJ Takahashi, CM Landowski, pp. 1-64. Reston, VA: US Geol. Surv.
- Townsend M, Huang M. 2022. Timescales of dike growth and chamber deflation constrain magma storage and transport pathways during Kīlauea's 2018 Lower East Rift Zone intrusion. J. Geophys. Res. Solid Earth 127(12):e2022JB025636
- Vinet N, Higgins MD. 2010. Magma solidification processes beneath Kilauea Volcano, Hawaii: a quantitative textural and geochemical study of the 1969-1974 Mauna Ulu lavas. J. Petrol. 51(6):1297-332
- Wadsworth FB, Llewellin EW, Farquharson JI, Gillies JK, Loisel A, et al. 2022. Crowd-sourcing observations of volcanic eruptions during the 2021 Fagradalsfjall and Cumbre Vieja events. Nat. Commun. 13(1):2611
- Walker BH, Houghton BF, Llewellin EW. 2023. Coexisting Strombolian and Hawaiian activity during the 2018 fissure eruption of Kīlauea—implications for processes of weak explosions. 7. Volcanol. Geotherm. Res. 435:107754
- Wang K, MacArthur HS, Johanson I, Montgomery-Brown EK, Poland MP, et al. 2019. Interseismic quiescence and triggered slip of active normal faults of Kīlauea Volcano's south flank during 2001-2018. 7. Geophys. Res. Solid Earth 124:9780-94
- Wang T, Segall P, Hotovec-Ellis AJ, Anderson KR, Cervelli PF. 2023. Ring fault creep drives volcano-tectonic seismicity during caldera collapse of Kīlauea in 2018. Earth Planet. Sci. Lett. In press
- Wang T, Zheng Y, Pulvirenti F, Segall P. 2021. Post-2018 caldera collapse re-inflation uniquely constrains Kīlauea's magmatic system. J. Geophys. Res. Solid Earth 126(6):e2021JB021803
- Wang TA, Coppess KR, Segall P, Dunham EM, Ellsworth W. 2022. Physics-based model reconciles caldera collapse induced static and dynamic ground motion: application to Kīlauea 2018. Geophys. Res. Lett. 49(8):e2021GL097440
- Wei X, Shen Y, Caplan-Auerbach J, Morgan JK. 2022. An improved earthquake catalog during the 2018 Kīlauea eruption from combined onshore and offshore seismic arrays. Earth Space Sci. 9(6):e2021EA001979
- Wieser PE, Edmonds M, Gansecki C, Maclennan J, Jenner FE, et al. 2022. Explosive activity on Kīlauea's lower East Rift Zone fueled by a volatile-rich, dacitic melt. Geochem. Geophys. Geosyst. 23(2):e2021GC010046
- Wieser PE, Edmonds M, Maclennan J, Jenner FE, Kunz BE. 2019. Crystal scavenging from mush piles recorded by melt inclusions. Nat. Commun. 10(1):5797
- Wieser PE, Lamadrid H, Maclennan J, Edmonds M, Matthews S, et al. 2021. Reconstructing magma storage depths for the 2018 Kīlauean eruption from melt inclusion CO2 contents: the importance of vapor bubbles. Geochem. Geophys. Geosyst. 22(2):e2020GC009364
- Wilding JD, Zhu W, Ross ZE, Jackson JM. 2023. The magmatic web beneath Hawai'i. Science 379(6631):462-68
- Anderson et al.



- Williams DM, Avery VF, Coombs ML, Cox DA, Horwitz, et al. 2020. U.S. Geological Survey 2018 Kilauea Volcano eruption response in Hawai'i-after-action review. Open File Rep. 2020-1041, US Geol. Surv., Reston, VA. https://doi.org/10.3133/ofr20201041
- Wolfe CJ, Solomon SC, Laske G, Collins JA, Detrick RS, et al. 2009. Mantle shear-wave velocity structure beneath the Hawaiian hot spot. Science 326(5958):1388-90
- Wright TL, Fiske RS. 1971. Origin of the differentiated and hybrid lavas of Kilauea Volcano, Hawaii. J. Petrol. 12(1):1-65
- Wright TL, Helz RT. 1996. Differentiation and magma mixing on Kilauea's east rift zone: a further look at the eruptions of 1955 and 1960. Part II. The 1960 lavas. Bull. Volcanol. 57(8):602-30
- Wright TL, Klein FW. 2014. Two hundred years of magma transport and storage at Kīlauea Volcano, Hawai'i. Prof. Pap. 1806, US Geol. Surv., Reston, VA. https://doi.org/10.3133/pp1806
- Wu S, Lin F, Farrell J, Shiro B, Karlstrom L, et al. 2020. Spatiotemporal seismic structure variations associated with the 2018 Kīlauea eruption based on temporary dense geophone arrays. Geophys. Res. Lett. 47(9):e2019GL086668
- Zoeller MH, Perroy RL, Wessels R, Fisher GB, Robinson JE, et al. 2020. Geospatial database of the 2018 lower East Rift Zone eruption of Kīlauea Volcano, Hawaii. Data release: US Geol. Surv., Reston, VA. https://doi. org/10.5066/P9S7UQKQ

